universe

IMPACT FACTOR 2.9

CITESCORE 3.6

Article

The Shock Cone Instabilities and Quasi-Periodic Oscillations around the Hartle–Thorne Black Hole

Orhan Donmez and Fatih Dogan

MDPI

https://doi.org/10.3390/universe10040152

universe

MDPI

Article

The Shock Cone Instabilities and Quasi-Periodic Oscillations around the Hartle–Thorne Black Hole

Orhan Donmez * and Fatih Dogan

College of Engineering and Technology, American University of the Middle East, Egaila 54200, Kuwait; fatih.dogan@aum.edu.kw

* Correspondence: orhan.donmez@aum.edu.kw

Abstract: To explain the observed X-ray data in a black hole–accreting matter system and understand the physical mechanisms behind QPOs, we have numerically modeled the dynamical and oscillation properties of the shock cone formed around both slowly and rapidly rotating Hartle–Thorne black holes, resulting from the mechanism of Bondi–Hoyle–Lyttleton (BHL). According to the numerical simulations, an increase in the quadrupole parameter leads to a decrease in the shock cone opening angle around the black hole. A larger quadrupole parameter results in more matter falling into the black hole within the cone. The combination of the quadrupole parameter and black hole rotation causes the matter inside the cone to exhibit chaotic motion. These dynamical changes and chaotic behavior of the shock cones excite the fundamental oscillation modes. Moreover, new frequencies have been formed due to the nonlinear coupling of the fundamental modes. Conversely, we have numerically studied the behavior of cones formed around rapidly rotating Hartle–Thorne black holes and found differences and similarities to those obtained from slowly rotating cases. Finally, comparing the outcomes obtained from Hartle–Thorne gravity with the results from Kerr and Einstein–Gauss–Bonnet (EGB) gravities reveals the impact of the quadrupole parameter on the shock cone and QPOs.

Keywords: numerical relativity; rotating black hole; alternative gravities; BHL; QPOs

Citation: Donmez, O.; Dogan, F. The Shock Cone Instabilities and Quasi-Periodic Oscillations around the Hartle–Thorne Black Hole. *Universe* **2024**, *10*, 152. https://doi.org/10.3390/universe10040152

Academic Editor: Daniela Doneva

Received: 2 March 2024
Revised: 15 March 2024
Accepted: 20 March 2024
Published: 24 March 2024

1. Introduction

One of the keys to unraveling the mysteries of the universe is to fully understand the nature and age of black holes and neutron stars. In this context, interpreting observed *X*-ray data is crucial for understanding these enigmatic objects. X-ray binary systems are among the most important sources of X-rays. In these systems, the compact object at the center emits X-rays while pulling material from the donor star and forming an accretion disk. If the compact object is a black hole, these observed X-rays could help reveal the characteristics of these mysterious structures in the universe.

In black hole X-ray systems, the gravitational attraction of the black hole draws matter from the donor star towards the black hole. This process initiates the formation of an accretion disk around the black hole. The interaction between the newly formed disk and the black hole leads to high X-ray luminosity. The period of this emission can vary from a few days to a few months [1]. The formation of X-rays could be attributed to instabilities and quasi-stable states in the disk. Transitions between these states can lead to the formation of quasi-periodic oscillations (QPOs) on the disk. Understanding the mechanisms behind these QPOs can contribute to our knowledge of the dynamic structure of the disk and to estimating the physical properties of the black hole at the center, such as its spin and mass. This information can provide answers to fundamental questions in astrophysics, leading to a better understanding of the universe.

In black hole X-ray binary systems, QPOs are divided into two categories: low-frequency and high-frequency QPOs. Low-frequency QPOs typically have a frequency of less than 30 Hz and are further classified into types A, B, or C based on their distinct

characteristics. High-frequency QPOs, on the other hand, are characterized by frequencies greater than 30 Hz [2]. These low- and high-frequency QPOs can create nonlinear combinations, resulting in emissions at various frequencies [2,3]. Over the past twenty years, thanks to the improved sensitivity of detectors, there has been a significant increase in the number of these observations. Spectral analysis of X-ray data from various sources has revealed the characteristics of many low- and high-frequency sources. Some notable examples include GRO J1655-40 with frequencies observed at 300 Hz and 450 Hz [4], XTE J1550-564 with frequencies ranging from 102 to 284 Hz [5], and GRS 1915+105 with frequencies observed between 67 Hz and 170 Hz [6], among others. It has also been observed that these frequencies often exhibit resonances, such as 3:2 and 5:3 ratios [7], and such resonant states are commonly observed in QPOs. These observations contribute significantly to our understanding of the dynamics of black hole systems and the physics of accretion disks. The resonances and varied frequencies of QPOs help in probing the inner regions of these disks and offer insights into the properties of the black holes themselves, such as their mass and spin.

The numerical solution of general relativistic hydrodynamic equations plays a crucial role in understanding the origin of QPOs in the vicinity of black holes [8–13]. By solving these equations, researchers can explore the dynamic structure of the accretion disk around black holes, the presence of shock waves, and other chaotic conditions that arise in regions close to the black hole event horizon, where gravity is extremely strong [14–25]. Low- and high-frequency QPOs, significant phenomena observed in these systems, have been a subject of extensive research in the literature [4,26–28]. By examining these QPOs, scientists aim to gain deeper insights into the complex dynamics of accretion disks and the influence of the strong gravitational field of black holes [3,29]. These studies involve analyzing how matter behaves in the extreme conditions near the black hole, including how it orbits, the speeds it reaches, and the ways in which it emits radiation (like X-rays) as it falls into the black hole. Understanding the generation and characteristics of these QPOs not only helps in probing the environment near black holes [25] but also provides valuable information about the properties of the black holes themselves, such as their mass, spin, and the nature of their gravitational pull [30–34].

To contribute to the explanation of observational data of compact objects and to investigate the source of electromagnetic emissions occurring around them, it is important to understand the cause of the mass increase around these objects. One of the cases leading to this mass increase is BHL accretion [35,36]. Initially proposed by Bondi and Hoyle, and later developed by Lyttleton, this mass accumulation mechanism occurs as a result of the movement of the compact object in the environment. Matter falling onto the moving compact object begins to accumulate towards the other side due to the strong gravitational attraction force and the velocity of the matter, thus forming a disk. Generally, as a result of BHL, shock cones or bow shocks form around black holes. Through these mechanisms, continuous accretion of matter onto the black hole is ensured, while also causing an increase in the mass of the black hole. The formulation of the BHL accretion mechanism can be found in work by Edgar [37], Giulini [38]. BHL accretion is important in explaining the nature of QPOs (quasi-periodic oscillations) formed in regions near the horizon where strong gravitational attraction forces, similar to black holes, predominate.

BHL accretion serves as a key process in forming either quasi-stable or stable accretion disks around black holes. This phenomenon occurs when matter is drawn from an upstream region into the black hole. The subsequent shock waves and physical events within these accretion disks provide insights into the mechanisms behind the phenomena observed in X-ray binary systems and active galactic nuclei (AGN). Extensively referenced in astrophysical research, this accretion process is crucial in the formation of disks around various black holes, including Schwarzschild [14,15,19,23,39,40], Kerr [16–18,21,41–43], and other types of black holes [24,44], facilitated by theoretical [37] and numerical applications of general relativistic hydrodynamics (GRH) and magnetohydrodynamics (MHD). An important observation from these studies is the formation of stable shock cones, which are

instrumental in generating X-ray emissions near black holes and lead to the occurrence of QPOs.

Numerical modeling of accretion disks and uncovering the resulting physical mechanisms would contribute to explaining some observational data. Studying these models using different gravities obtained from solving the Einstein equations would aid in comparing the numerical data with observational data and understanding the nature of the X-rays emitted in such astrophysical events. One of these gravities is Hartle–Thorne. The Hartle–Thorne metric describes the geometry in the region where the gravitational field of a slowly rotating and slightly deformed compact object is strong. This metric is defined based on three different multipole moments: the mass, rotation, and quadrupole parameters of the compact object [45,46]. The Hartle–Thorne solution not only describes the spacetime outside the compact object but also defines the gravitational field inside it. Hartle–Thorne gravity has a more general solution compared to Kerr [45,47]. While the Kerr solution is only applicable to rotating black holes, the Hartle–Thorne solution can be applied to a wide range of compact objects. On the other hand, since the Hartle–Thorne metric includes the quadrupole parameter due to the deformation of the rotating object, variations in spacetime with this parameter provide explanations for different astrophysical phenomena. The Hartle–Thorne solution approaches the Kerr solution in the case of slow rotation of the compact object. Thus, it can be used in scenarios involving slowly rotating black holes [48–50]. Describing the spacetime around the black hole with the Hartle–Thorne metric could lead to alternative solutions to events, such as understanding the mass accretion scenarios around these objects and uncovering different physical mechanisms that may occur.

We use BHL accretion to describe the structure of the shock cone around both slowly and rapidly rotating Hartle–Thorne black holes. This allows us to determine the physical characteristics of the resulting shock waves and the QPO oscillation frequencies, all in relation to the quadrupole moment (q) of Hartle–Thorne gravity. We also compare our findings with previous studies and models of Schwarzschild, Kerr, and EGB black holes, revisited here based on the spin parameter of the black hole used in this paper. This comparison highlights how the shock wave properties differ in the context of Hartle–Thorne gravity. Our focus is on examining how this gravity, originally formulated for slowly rotating compact objects [50,51], interacts with the matter surrounding a rapidly rotating black hole. This investigation aims to understand the dynamics of such systems under the influence of gravity in rapidly rotating conditions. Finally, we shed light on how observational data can be explained using QPOs derived from all these gravities, focusing particularly on the novel contributions of Hartle–Thorne gravity in this field.

In this article, all calculated physical parameters vary depending on the mass of the central black hole. This variability allows the calculations to explain the X-ray data observed in systems with either stellar-mass or supermassive black holes. If the mass of the central black hole is the only known parameter, it can be used in geometrized units to express the rest-mass density, mass accretion rate, oscillation frequency, and other parameters in the SI unit system. Throughout the paper, unless explicitly stated otherwise, we adopt the convention of using geometrized units, where c and G are set to 1.

2. Equations

2.1. Hartle–Thorne Spacetime Metric

The existing studies on the physical properties of the shock cone formed around black holes, using Schwarzschild and Kerr geometries, are important for understanding one aspect of the universe nature. However, these models are somewhat limited. The Hartle–Thorne model not only incorporates the rotation parameter of the black hole into the calculations but also accounts for the effects of the quadrupole parameter. Thus, by presenting a more general and realistic model, it can reveal the physical properties of the shock cone around black holes more accurately. The data obtained from the Hartle–Thorne black

hole model can be used to explain the physical reasons behind observational data taken from complex astrophysical systems.

The Hartle–Thorne metric is one of the solutions of General Relativity that describes the spacetime around a rotating compact object with static and axial symmetry. This metric, resulting from the rotation of the object, extends the geometry by including small distortions in the surrounding spacetime, known as the quadrupole parameter, going a step beyond the Kerr black hole. Particularly applied to slowly rotating neutron stars [48,49], this metric can also be applied to black holes [48,50], allowing for different modeling of the compact object gravitational field. The quadrupole parameter is, in fact, a result of the shape change caused by the rotation of the compact object.

The Hartle–Thorne metric describes the spacetime around slowly rotating black holes, and this description depends on the parameters of the mass quadrupole moment Q and angular momentum $(a = J/M^2)$. The dimensionless quadrupole moment parameter is defined as $(q = Q/M^3)$ This metric has been developed as a solution to the Einstein field equations in a vacuum, taking into account the mass, angular momentum, and mass quadrupole moment of the black hole. The Hartle–Thorne metric includes calculations up to the second order of angular momentum and the first order of the mass quadrupole moment, allowing for a detailed examination of the spacetime around black holes within the Theory of General Relativity. The Hartle–Thorne spacetime metric is cited in [50,51] as:

$$\begin{aligned} ds^2 = &-\left(1-\frac{2M}{r}\right)\left(1+2f_1P_2(Cos\theta)+2\left(1-\frac{2M}{r}\right)^{-1}\frac{J^2}{r^4}\left(2Cos^2\theta-1\right)\right)dt^2 \\ &+\left(1-\frac{2M}{r}\right)^{-1}\left(1-2f_2P_2(Cos\theta)-2\left(1-\frac{2M}{r}\right)^{-1}\frac{J^2}{r^4}\right)dr^2 \\ &-\frac{4J}{r}Sin^2\theta dtd\phi+r^2[1-2f_3P_2(Cos\theta)]d\theta^2 r^2[1-2f_3P_2(Cos\theta)]Sin^2\theta d\phi^2, \end{aligned} \tag{1}$$

where $P_2(Cos\theta) = \frac{1}{2}(3Cos^2\theta - 1)$, $f_1 = \frac{J^2}{Mr^3}\left(1+\frac{M}{r}\right) + \frac{5}{8}\frac{Q-J^2/M}{M^3}Q_2^2(\frac{r}{M}-1)$, $f_2 = f_1 - \frac{6J^2}{r^4}$, $f_3 = f_1 + \frac{J^2}{r^4} + \frac{5}{4}\frac{Q-J^2/M}{M^2(r^2-2Mr)^{1/2}}Q_2^1(\frac{r}{M}-1)$. $P_2(Cos\theta)$ is the second Legendre polynomial of the first kind. Q_2^1 and Q_2^2 are the associated Legendre polynomials of the second kind which are $Q_2^1 = (x^2-1)^{1/2}\left(\frac{3x}{2}ln\frac{x+1}{x-1} - \frac{3x^2-2}{x^2-1}\right)$ and $Q_2^2 = (x^2-1)\left(\frac{3}{2}ln\frac{x+1}{x-1} - \frac{3x^3-5x}{x^2-1}^2\right)$ as a function of x which is $x = \frac{r}{M} - 1$.

The Hartle–Thorne metric, which is an extension of the Schwarzschild metric, incorporates the effect of the rotation parameter and describes the spacetime around black holes. Figure 1 illustrates the variation in the horizon of the Hartle–Thorne black hole with respect to the black hole rotation parameter. As seen in the figure, the smallest horizon occurs at $q = 0$ where $r = 2M$. For $q > 0$, it is observed that the horizon moves away from $2M$. On the other hand, the black hole rotation parameter slightly decreases the size of the horizon. In other words, at the same q, the horizon approaches $2M$ slightly. This demonstrates that the Hartle–Thorne metric behaves similarly to the Kerr metric [50].

To address the GRH equations within the spacetime matrix, it is necessary to establish the lapse function and shift vectors within the Hartle–Thorne coordinate framework. The connection between the four-dimensional metric g_{ab} and the three-dimensional metric γ_{ij}, along with the lapse function and shift vectors, is described as follows [52]:

$$\begin{pmatrix} g_{tt} & g_{ti} \\ g_{it} & \gamma_{ij} \end{pmatrix} = \begin{pmatrix} (\beta_k\beta^k - \alpha^2) & \beta_k \\ \beta_i & \gamma_{ij} \end{pmatrix}, \tag{2}$$

where $i, j, k = 1, 2$ and 3, the lapse function for Hartle–Thorne spacetime metric is

$$\alpha = \sqrt{\frac{4J^2}{r^4(1+f3)} - \left(1 - f_1 - \frac{2J^2}{r^4\left(1-\frac{2M}{r}\right)}\right)\left(\frac{2M}{r} - 1\right)}, \tag{3}$$

and the shift vectors can be represented as

$$\beta_r = 0, \quad \beta_\theta = 0, \quad \beta_\phi = -\frac{2J}{r}. \tag{4}$$

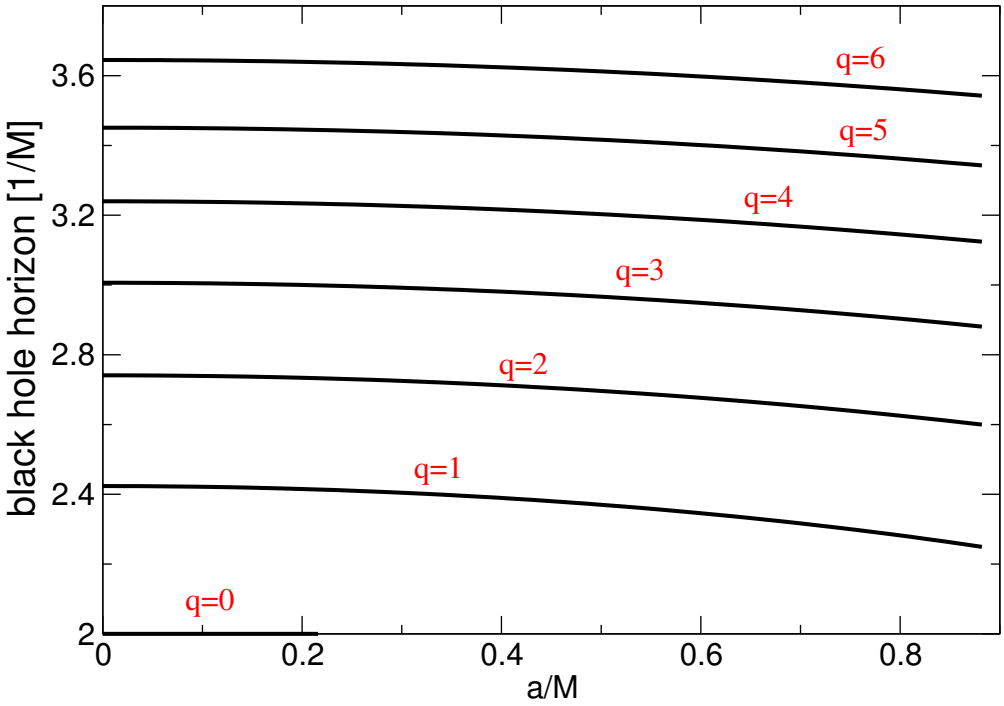

Figure 1. The variation in the horizon of the Hartle–Thorne black hole is dependent on both the black hole rotation parameter and quadrupole moment. As q increases, the horizon moves further away from $2M$, while as a/M increases, it approaches $2M$ slightly.

2.2. EGB and Kerr Spacetime Matrices

Four-dimensional Einstein–Gauss–Bonnet gravity, as proposed by Glavan and Lin [53], Ghosh and Kumar [54], represents a significant advancement in gravitational theory that describes the spacetime around black holes by bypassing Lovelock theorem. It is entirely independent of Ostrogradsky instability. Initially, this theory delineates the geometry of a static, spherically symmetric black hole, which, unlike the Schwarzschild black hole, features two horizons instead of one, determined by the EGB constant. A rotating EGB black hole model has also been introduced [24,55]. Despite ongoing debates in the scientific community regarding its validity, there have been efforts to apply it both numerically and theoretically to various astrophysical systems to derive solutions. This black hole model, offering an alternative solution that depends on the EGB coupling constant beyond the Schwarzschild and Kerr black holes, plays a crucial role in spherically symmetric systems to unravel the universe's mysteries. Further details about EGB black holes can be found in Donmez [24], Glavan and Lin [53], Ghosh and Kumar [54], Donmez et al. [56], and their cited works.

EGB gravity presents a unique alternative to traditional gravitational theories by offering distinct solutions within the framework of Einstein equations [57]. This theory is distinguished by its inclusion of an alpha (α) parameter, which is absent in Kerr gravity, which defines the gravitational field around the rotating black hole. The impact of the α parameter becomes particularly significant in regions close to black holes, serving as a crucial tool for elucidating various observed astronomical phenomena. By including

terms of a higher order in curvature than those found in General Relativity, the α parameter enriches our understanding of black hole behavior under extreme conditions and within the context of higher-dimensional spacetime. The metric for EGB is detailed in [24,54,56].

$$\begin{aligned} ds^2 &= -\frac{\Delta_2 - a^2 sin^2\theta}{\Sigma} dt^2 + \frac{\Sigma}{\Delta_2} dr^2 - 2asin^2\theta \left(1 - \frac{\Delta_2 - a^2 sin^2\theta}{\Sigma}\right) dt d\phi + \Sigma d\theta^2 + \\ & sin^2\theta \left[\Sigma + a^2 sin^2\theta \left(2 - \frac{\Delta_2 - a^2 sin^2\theta}{\Sigma}\right)\right] d\phi^2, \end{aligned} \tag{5}$$

where $\Sigma = r^2 + a^2 \cos^2\theta$, $\Delta_2 = r^2 + a^2 + \frac{r^4}{2\alpha}\left(1 - \sqrt{1 + \frac{8\alpha M}{r^3}}\right)$. Within this framework, the variables M, α, and a represent the black hole mass parameter, the Gauss–Bonnet coupling constant, and the black hole spin, respectively. The lapse function is given by $\tilde{\alpha} = \sqrt{\frac{a^2(1-f(r))^2}{r^2 + a^2(2-f(r))} + f(r)}$, while the shift vectors are defined as $\beta^i = \left(0, 0, \frac{ar^2}{2\pi\alpha}\left(1 - \sqrt{1 + \frac{8\pi\alpha M}{r^3}}\right)\right)$. The function $f(r)$ is determined by the expression $f(r) = 1 + \frac{r^2}{2\alpha}\left(1 - \sqrt{1 + \frac{8\alpha M}{r^3}}\right)$. In the GRH equations, the gamma matrix, symbolized as $\gamma_{i,j}$, outlines the three-dimensional space. It is extracted from the metrics g_{ab} applicable to both Kerr and EGB gravities. Here, the Latin indices i and j range from 1 to 3.

The gravitational force of the Kerr black hole is very strong due to its rotation parameter, which significantly warps the surrounding spacetime. This effect is particularly important when exploring the properties of accreting matter in the inner area, where the Kerr metric is the most suitable tool for analysis. The metric of the Kerr black hole, expressed in Boyer–Lindquist coordinates, is defined as follows [16,52].

$$ds^2 = -\left(1 - \frac{2Mr}{\sum^2}\right) dt^2 - \frac{4Mra}{\sum^2} sin^2\theta dt d\phi + \frac{\sum^2}{\Delta_1} dr^2 + \sum^2 d\theta^2 + \frac{A}{\sum^2} sin^2\theta d\phi^2, \tag{6}$$

where $A = (r^2 + a^2)^2 - a^2 \Delta sin^2\theta$ and $\Delta_1 = r^2 - 2Mr + a^2$. The shift vector and lapse function of the Kerr metric are given by shift vector (β^i): $\beta^t = 0$, $\beta^r = 0$, and $\beta^\theta = \frac{-2Mar}{A}$. The lapse function is $\tilde{\alpha} = \sqrt{\frac{\Delta_1}{A}}$.

2.3. General Relativistic Hydrodynamic Equations

Modeling the shock cone around black holes, formed as a result of BHL accretion using different gravitational theories, can lead to various physical processes on the cone and also to the formation of different QPO frequencies. In this article, to model the shock cone around Kerr, EGB, and Hartle–Thorne black holes, we numerically solved two-dimensional, General-Relativity-based hydrodynamic equations on the equatorial plane in an ideal fluid state, neglecting the effect of the magnetic field. The conserved form of the GRH equations is given as follows [58,59]:

$$\frac{\partial U}{\partial t} + \frac{\partial F^r}{\partial r} + \frac{\partial F^\phi}{\partial \phi} = S. \tag{7}$$

The vectors U, F^r, F^ϕ, and S are associated with the conserved variables, the fluxes in the r and ϕ directions, and the source terms, respectively. These conserved variables are determined based on the primitive variables, as demonstrated in the following description:

$$U = \begin{pmatrix} D \\ S_j \\ \tau \end{pmatrix} = \begin{pmatrix} \sqrt{\gamma} W \rho \\ \sqrt{\gamma} h \rho W^2 v_j \\ \sqrt{\gamma}(h\rho W^2 - P - W\rho), \end{pmatrix} \tag{8}$$

and the fluxes are

$$\vec{F}^i = \begin{pmatrix} \tilde{\alpha}\left(v^i - \frac{1}{\tilde{\alpha}\beta^i}\right) D \\ \tilde{\alpha}\left(\left(v^i - \frac{1}{\tilde{\alpha}\beta^i}\right) S_j + \sqrt{\gamma} P \delta^i_j\right) \\ \tilde{\alpha}\left(\left(v^i - \frac{1}{\tilde{\alpha}\beta^i}\right) \tau + \sqrt{\gamma} P v^i\right) \end{pmatrix} \tag{9}$$

and,

$$\vec{S} = \begin{pmatrix} 0 \\ \tilde{\alpha}\sqrt{\gamma} T^{ab} g_{bc} \Gamma^c_{aj} \\ \tilde{\alpha}\sqrt{\gamma}\left(T^{a0}\partial_a \tilde{\alpha} - \tilde{\alpha} T^{ab} \Gamma^0_{ab}\right) \end{pmatrix} \tag{10}$$

where Γ^c_{ab} is the Christoffel symbol, $h = 1 + \epsilon + P/\rho$ represents the enthalpy, $W = (1 - \gamma_{a,b} v^i v^j)^{1/2}$ denotes the Lorentz factor, and $v^i = u^i/W + \beta^i$ represents the three-velocity of the fluid. ϵ, $\gamma_{i,j}$, γ, g^{ab}, ρ, u^a, p, and h are the internal energy, the three-metric which defines the space curvature, the determinant of the three-metric, the four-metric of the curved spacetime, the rest-mass density, the four-velocity of the fluid, the fluid pressure, and the specific enthalpy, respectively. The indices a, b, and c range from 0 to 3.

3. Initial and Boundary Conditions

BHL accretion describes a mass accretion mechanism that occurs as a result of matter from the interstellar environment falling towards the black hole due to the movement of the black hole at the center. We model the shock cone formed by the matter falling towards the black hole from one side of a spherical surface by numerically solving the hydrodynamic equations of the General Theory of Relativity, thereby trying to understand the mechanism of the accreting matter and the physical properties of the shock cone. In this paper, while doing this, we use different gravities to understand the parameters that are effective in that gravity for the formation of the shock cone and the characteristics of the QPO frequencies that occur in the meantime. For numerical modeling, we define the density of the matter falling towards the black hole as $\rho = 1$. We calculate the pressure of the falling matter using the ideal gas equation $P = (\Gamma - 1)\rho\epsilon$ with the speed of sound $C_\infty = 0.1$. Here, the adiabatic index is $\Gamma = 4/3$. Also, the radial, $V^r = \sqrt{\gamma^{rr}} V_\infty \cos(\phi)$, and angular, $V^\phi = -\sqrt{\gamma^{\phi\phi}} V_\infty \sin(\phi)$, velocities defined in BHL accretion have been used. As seen, these velocities are defined depending on the gas asymptotic speed V_∞. The dependence of the shock cone on the asymptotic speeds in different gravities is explained in [14,16,17,19,21,39–42,44,56]. The matter is sent to the computational domain with the defined density, pressure, and velocities from the outer boundary, thereby forming the shock cone and its instabilities using an asymptotic $V_\infty = 0.2$. Here, the value $V_\infty = 0.2$ is defined as the most effective asymptotic speed value for producing QPOs according to [16,17,56]. Other parameters required for these models are summarized in Table 1.

In our simulation, the computational grid is arranged with equal spacing in both radial and angular directions. This setup includes $N_r = 1024$ cells radially and $N_\phi = 256$ cells angularly. The simulation space radial boundaries are set at $r_{min} = 3.7\ M$ for the inner boundary and $r_{max} = 100M$ for the outer boundary. Angularly, the boundaries are determined at $\phi_{min} = 0$ and $\phi_{max} = 2\pi$.

The simulation duration ($t_{max} = 35{,}000\ M$) extends well beyond the time required for the shock cone to reach a steady state, including the development of a steady shock cone. It is observed that the primary features of the simulation results, including the occurrence of QPOs, the development of instabilities, the occurrence of shock waves, and the trends in accretion rates, are not significantly affected by changes in grid resolution [24,44,56].

The correct treatment of boundaries is essential in numerical simulations to prevent unrealistic results. For the inner boundary, we apply an outflow boundary condition to allow the gas to fall into the black hole through straightforward zeroth-order extrapolation. At the outer boundary, gas is consistently injected with the initially mentioned density, velocities, and pressure in the upstream region of the computational domain, and an

outflow boundary condition is employed on the downstream side of the computational domain. Along the ϕ-direction, periodic boundary conditions are employed to maintain the continuous behavior of the simulation.

Table 1. The initial model adopted for the numerical simulation of Kerr, Gauss–Bonnet, and Hartle–Thorne metrics. *Model*, *type*, α, a/M, q, and τ_{ss} are the name of the model, gravity, Gauss–Bonnet coupling constant, black hole rotation parameter, quadrupole parameter, and time required to reach the steady state, respectively.

Model	*Type*	$\alpha(M^2)$	a/M	q	τ_{ss}/M
SCH	*Schwarzschild*	–	–	–	3100
*K*04	*Kerr*	–	0.4	–	2600
*K*09		–	0.9	–	2350
*K*0_*EGB*1	*Gauss-Bonnet*	0.63	0	–	3500
*K*0_*EGB*2		−3.7	0	–	3200
*K*04_*EGB*1		0.63	0.4	–	3100
*K*04_*EGB*2		−3.89	0.4	–	2900
*K*09_*EGB*1		0.054	0.9	–	2600
*K*09_*EGB*2		−3.61	0.9	–	2400
*K*04_*HT*1	*Hartle-Thorne*	–	0.4	0	2400
*K*04_*HT*2		–	0.4	0.5	2550
*K*04_*HT*3		–	0.4	1	2700
*K*04_*HT*4		–	0.4	2	2800
*K*04_*HT*5		–	0.4	3	2900
*K*04_*HT*6		–	0.4	4	3000
*K*04_*HT*7		–	0.4	5	3100
*K*09_*HT*1	*Hartle-Thorne*	–	0.9	0	2200
*K*09_*HT*2		–	0.9	0.5	2250
*K*09_*HT*3		–	0.9	0.8	2230
*K*09_*HT*4		–	0.9	1	2800
*K*09_*HT*5		–	0.9	2	2900
*K*09_*HT*6		–	0.9	3	3000
*K*09_*HT*7		–	0.9	5	3200

4. BHL Accretion around a Slowly Rotating Black Hole in Hartle–Thorne Gravity: $a/M = 0.4$

This work aims to advance our theoretical understanding in astrophysics by providing significant insights into black holes and the dynamics of matter around them. Hartle–Thorne black holes, as an important application of General Relativity Theory, enable us to gain more information about these mysterious objects in the universe through such research.

The Hartle–Thorne metric is an extended version of the Schwarzschild metric, designed to understand the spacetime structure around slowly rotating black holes. The Hartle–Thorne solution can be applied to various scenarios involving rotating compact objects, such as neutron stars or black holes, regardless of whether the mass around the compact object is low or high. This metric takes into account the black hole rotational parameters and quadrupole moment, providing a more realistic spacetime model. In this context, studying the shock cones that form around slowly rotating black holes is crucial. Unlike the Kerr solution, the Hartle–Thorne metric examines the effects of quadrupole moments on QPOs in the shock cone formed around rotating black holes. This examination is critically important for understanding the QPO phenomena observed in high-energy astrophysics and X-ray timing. The Hartle–Thorne metric demonstrates how spacetime is warped around a rotating black hole, particularly how light bends near the surface of the black hole. This bending of light is vital for understanding the structure and dynamics of the shock cone around black holes. Additionally, understanding the effect of the quadrupole parameter on spacetime can contribute to explaining some unexplained

observational data. The numerical results obtained from this study aid in comprehending complex problems in high-energy astrophysics.

4.1. Dynamics of Shock Cones around a Hartle–Thorne Black Hole

In the vicinity of a slowly rotating Hartle–Thorne black hole, the behavior of the shock cone formed as a result of BHL accretion, according to the quadrupole parameter, is shown in Figure 2. Figure 2 demonstrates how the density, represented by color, contour lines, and a velocity vector plot on the equatorial plane, changes with the quadrupole parameter. A value of $q = 0$ emphasizes that near the horizon of the black hole, the mass distribution shows an ideal symmetric distribution, while $q = 5$ indicates a significant deviation from spherical symmetry in this distribution. As seen in Figure 2, the contour lines representing density undergo changes near the black hole, both inside and outside the shock cone. Especially inside the shock cone, the flattening of these lines has increased, indicating that, due to the influence of the quadrupole parameter, the situation has evolved from a spherically symmetric to an elliptical one. This change definitively affects the behavior of the QPOs trapped inside the shock wave. In addition to these, by drawing a velocity vector graph, we can see how matter falls into the black hole and how the shock cone continuously feeds on matter. Additionally, it has been observed that the stagnation point is formed at almost the same point ($r \sim 25\ M$) inside the shock cone in all models. In other words, as matter within the cone with $r < 25\ M$ falls towards the horizon of the black hole, it is also pushed outward. The continuously falling matter in a strong gravitational field can continuously generate X-ray emissions.

The location of the shock wave and the opening angle of the cone near the black hole horizon change the physical properties of the X-rays occurring in that area, and consequently, the QPO frequencies. Figure 3 shows how the dynamic structure of the shock cone, formed around the slowly rotating ($a/M = 0.4$) Hartle–Thorne black hole, changes with the quadrupole parameter. On the left side of the figure, the change in density with azimuthal length at $r = 3.88\ M$ is presented. The positions of the shock waves and the presence of the cone are clearly visible. The right part of the same figure illustrates the change in the opening angle of the formed shock cone depending on q. As seen in both graphs, the opening angle decreases as q increases. At the same time, the amount of matter within the cone also tends to decrease. These changes in the cone affect the physical properties of the X-rays and, thus, the QPOs generated by the interaction of the black hole with the shock cone. Moreover, the interaction of the stationary shock waves formed around the black hole leads to the formation of nonlinear chaotic behaviors. These behaviors cause the nonlinear coupling of the fundamental oscillation frequencies and lead to the formation of new observable modes.

The changes in the radial and angular velocities of the shock cone around black holes lead to alterations in the characteristic structure of the X-rays produced. In Figure 4, at $r = 3.88\ M$, the changes in the radial (see the left graph) and angular (see the right graph) velocities of the cone, and consequently the shock cone resulting from BHL accretion, are presented in relation to the quadrupole parameter. As observed in the right graph, at the boundaries of the shock cone, i.e., where the stationary shock waves are located, the matter falling towards the black hole slows down, while inside and outside the cone, the matter accelerates as it falls towards the black hole. Simultaneously, as seen in the left figure, where the radial velocity decreases at the shock waves, the angular velocity increases. The increase in radial velocity leads to a rise in the matter temperature and thus to the emission of high-energy X-rays. Simultaneously, the change in radial velocity at a fixed $r = 3.88\ M$ leads to variations in the observed X-rays and consequently changes in the QPO frequencies. On the other hand, the changes in angular velocity and high angular velocity cause broadening due to the Doppler effect. This broadening plays an effective role in the variations in X-rays at the boundaries of the shock cone. The formed shock cone and slowing shock waves lead to the formation of different QPO frequencies. They also contribute to chaotic behavior, which in turn helps in the generation of various QPO frequencies.

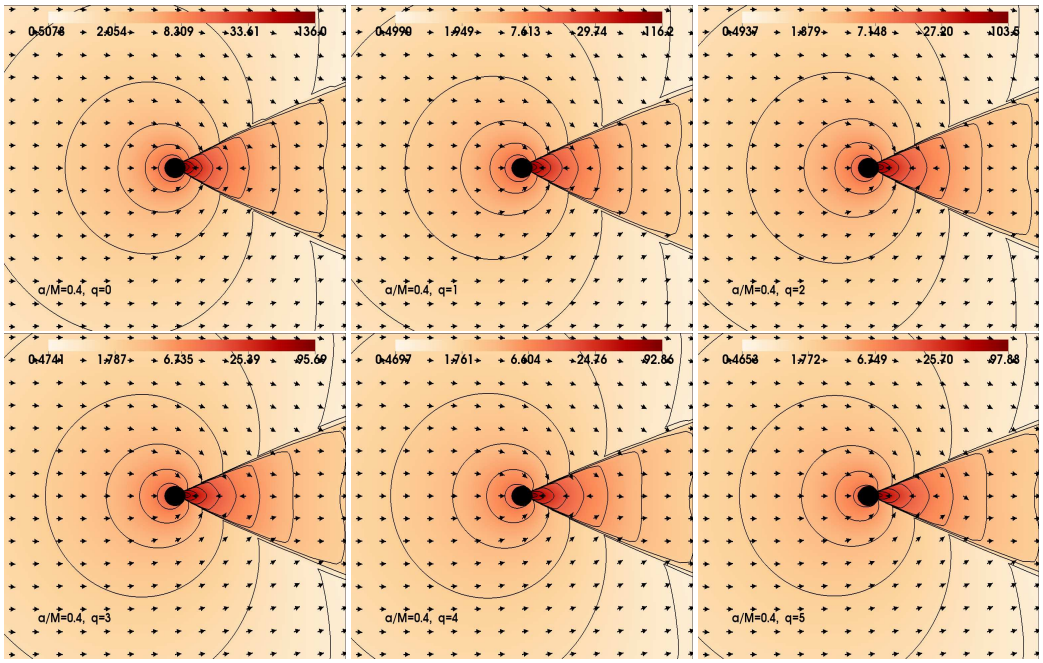

Figure 2. These snapshots refer to the variation in the logarithmic density and the structure of shock waves around the black hole with $a/M = 0.4$, depicted on the equatorial plane with color, contour lines, and a velocity vector plot. To observe the change in density and shock cones near the black hole horizon, and how they are affected by the Hartle–Thorne quadrupole parameter (q), the focus is on a region from $[x_{min}, y_{min}] \rightarrow [-60M, -60M]$ to $[x_{max}, y_{max}] \rightarrow [60\ M, 60\ M]$. This representation is plotted much later after the shock cone has reached a steady state, specifically around $t = 30{,}000\ M$. Particularly, the influence of q on the dynamics of the shock cone is clearly visible in the region near the black hole horizon, where the gravity is very strong. The influence of q on the dynamics of the shock cone is moderate (not strong), with changes in density from $\sim$136 to $\sim$93 and at shock opening angles from 1.2 to 0.9 *rad* for $q = 0$ to 5.

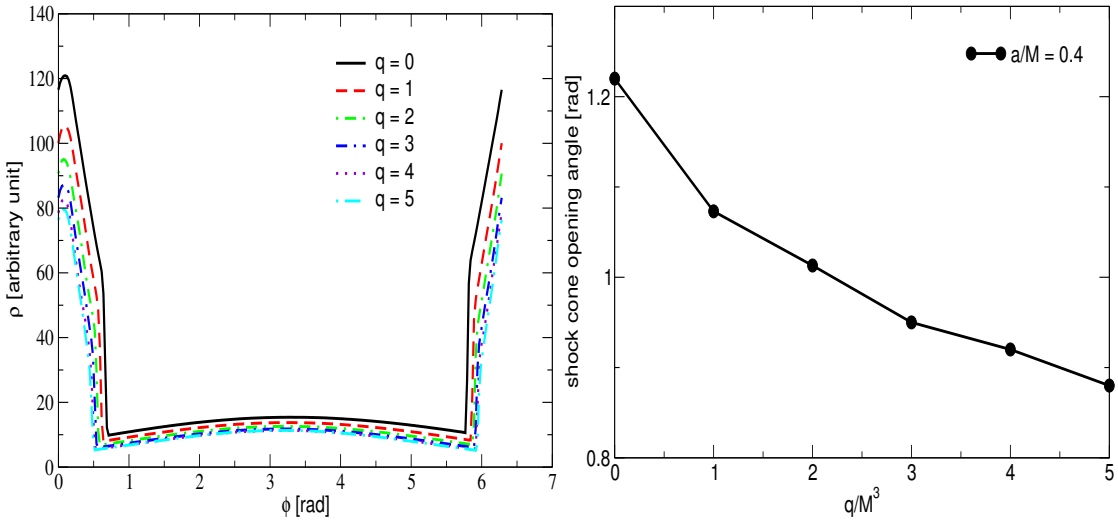

Figure 3. This figure depicts how the opening angle of the shock cone formed around the black hole with $a/M = 0.4$ changes depending on the value of the parameter q. It has been observed that q not only affects the amount of matter around the black hole and within the shock cone but also alters the cone opening angle. In both graphs presented, it is apparent that as the value of q increases, the opening angle of the cone decreases. This change in the cone opening angle, in turn, leads to variations in the trapped QPO frequencies within the cone. This phenomenon highlights the complex interplay between the physical parameters of the black hole and the dynamic properties of the matter and radiation in its vicinity.

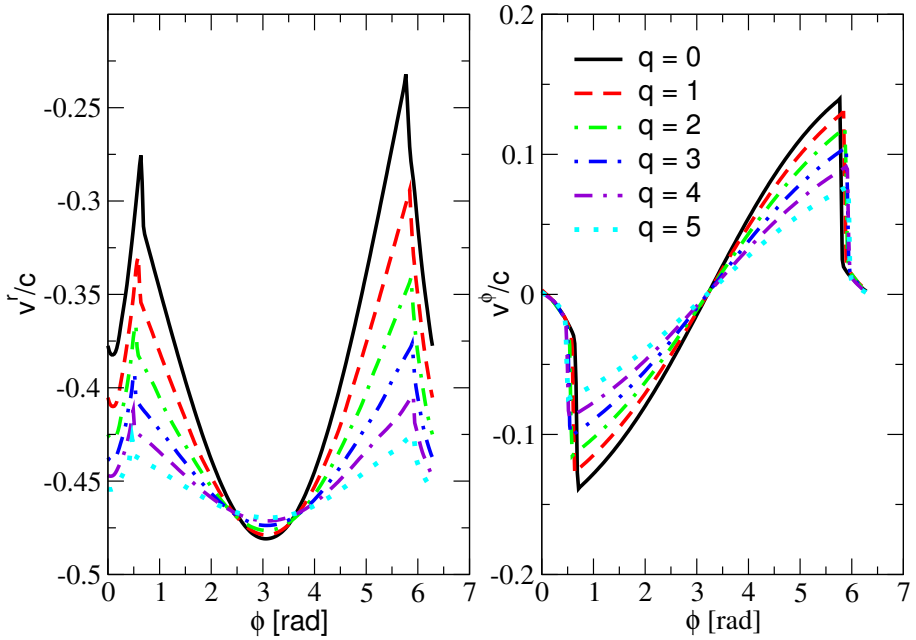

Figure 4. The variation in the radial and azimuthal velocities at a specific point, $r = 3.88\ M$, in relation to the azimuthal angle for $a/M = 0.4$. The left graph demonstrates how the radial velocity decreases at the location of the shock wave, indicating that the speed of matter falling towards the black hole is slowing down. On the other hand, the right graph shows that within the shock wave, the azimuthal velocity of the trapped matter is nearly zero. This essentially means that the matter is falling directly towards the black hole and accreting within the cone, without significant azimuthal (or tangential) movement. This observation is crucial in understanding the dynamics of matter in the vicinity of the black hole, especially how it behaves when influenced by shock waves and gravitational forces.

4.2. The Shock Cone Instability around the Hartle–Thorne Black Hole

The stability of the shock cone and the emergence of quasi-periodic behavior are crucial for revealing the physical characteristics of the cone and explaining the observed spectral data. In Figure 5, at $r = 3.88\ M$, the changes in the mass accretion rate and the behavior over time of the $m = 1$ mode after reaching saturation are considered for different quadrupole parameter scenarios. As observed in the left part of the figure, after the shock cone reaches a steady state, the mass accretion rate exhibits fluctuations around a certain value, indicating signs of instability even in the steady state. This phenomenon is noted for quadrupole values of $q = 3$ and below, while for higher values of q, either no significant change is observed or the changes are not as pronounced as for lower values. Particularly, for $q = 5$, the mass accretion exhibits a steady state without oscillations. On the other hand, as the value of q increases, the amount of matter falling into the black hole increases, leading to a decrease in the amount of matter in the shock cone. The right graph in Figure 5 illustrates the power of the mode, showing an increase in instability until it reaches a steady state and saturation around $t = 5000\ M$. From this point onwards, the shock cone maintains its steady state, indicating that different modes of QPO frequencies are regularly formed and propagated in such systems.

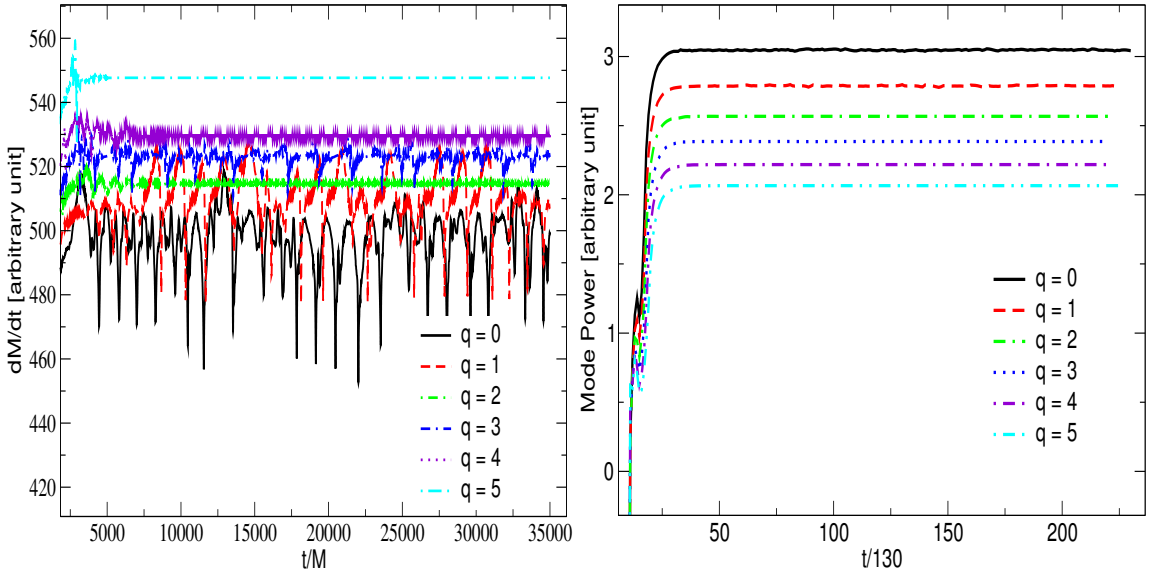

Figure 5. The changes in instability of the accreting matter and the resulting shock cone around the black hole with $a/M = 0.4$ after reaching the steady state, as related to the parameter q, are demonstrated. The left graph shows that at $r = 3.88\ M$, the mass accretion rate for certain q values continues to oscillate around an equilibrium point even after reaching the stable state. The right graph, however, indicates that each model reaches a stable state around the same time, approximately at $t = 4000\ M$.

4.3. QPOs around the Hartle–Thorne Black Hole

The instability of the shock cone around black holes, which is directly proportional to the instability of the mass accretion rate, seen in Figure 5, leads to the excitation of QPO modes. If the shock cone oscillates around a certain value after reaching saturation, it enables the observation of these modes through telescopes, as these modes can be continuously produced within the cone. The shock cone confines oscillation modes within itself and excites them, leading to the formation of QPOs. These modes arise due to pressure differences. According to our understanding and the literature [42,60], two different pressure modes are excited within the cone. These correspond to the frequencies generated by exciting the mode confined within the cone in the azimuthal direction, referred to as f_{sh}. This entirely depends on the shock cone opening angle. A smaller opening angle results in a higher oscillation frequency. On the other hand, the excitation of modes trapped in the radial direction between the stagnation point within the cone and the black hole horizon is referred to as f_{EH} In Figure 6, the instability formed around the slowly rotating Hartle–Thorne black hole is examined to reveal the QPO behaviors generated by these shock cones through a power spectrum analysis (PSD). We plot two different PSD lines for each value of q. The first one is obtained from the mass accretion rate acquired throughout the simulation time after the shock cone reaches the steady state (t∼2200 M). The other one, on the other hand, is calculated during the time span from well after the shock cone reached a stable state, specifically from t∼20,000 M to $t_{max} = 35{,}000\ M$. These two different PSD plots demonstrate that most of the frequencies formed within the cone are not transient but genuine modes, as mentioned above, after the shock cone reached the steady state. These modes continue to occur continuously afterward. In other words, as long as the shock cone exists and the same physical conditions are maintained, the same frequencies are consistently observed. The QPO frequencies arising within the shock cone, dependent on the quadrupole parameter, have been identified. As depicted in the figure, at each q value, QPO modes are observed to be trapped inside the cone, forming fundamental modes. These modes typically correspond to the first two peaks observed in each q. Additionally, due to the chaotic structure of the shock cone, these modes exhibit non-linear coupling or resonance conditions, resulting in the emergence of new frequencies.

Generally, these frequencies are observed to follow the 1:2:3... ratio, aligning with findings from observational studies. Notably, around $q = 1$, where the oscillation amplitude is high, the power of the frequencies is also significant, indicating that the frequencies in this scenario have higher observability. As a result, in the case of $a/M = 0.4$, $q = 1$ has the potential to explain observational data. The results obtained for this quadrupole parameter can be compared with the QPOs obtained from black hole observations to estimate not only the mass of the black hole but also its spin parameter. In conclusion, the shock cone formed around the Hartle–Thorne black hole, exhibiting rich oscillation characteristics, can be utilized to understand the physical properties of the black hole by comparing the results obtained here with observations. The PSD derived from the mass accretion rate data acquired long after the shock cone attained its steady state, along with the peaks marked by the dashed line in Figure 6, possesses characteristics suitable for comparison with observations and can be regarded as persistent.

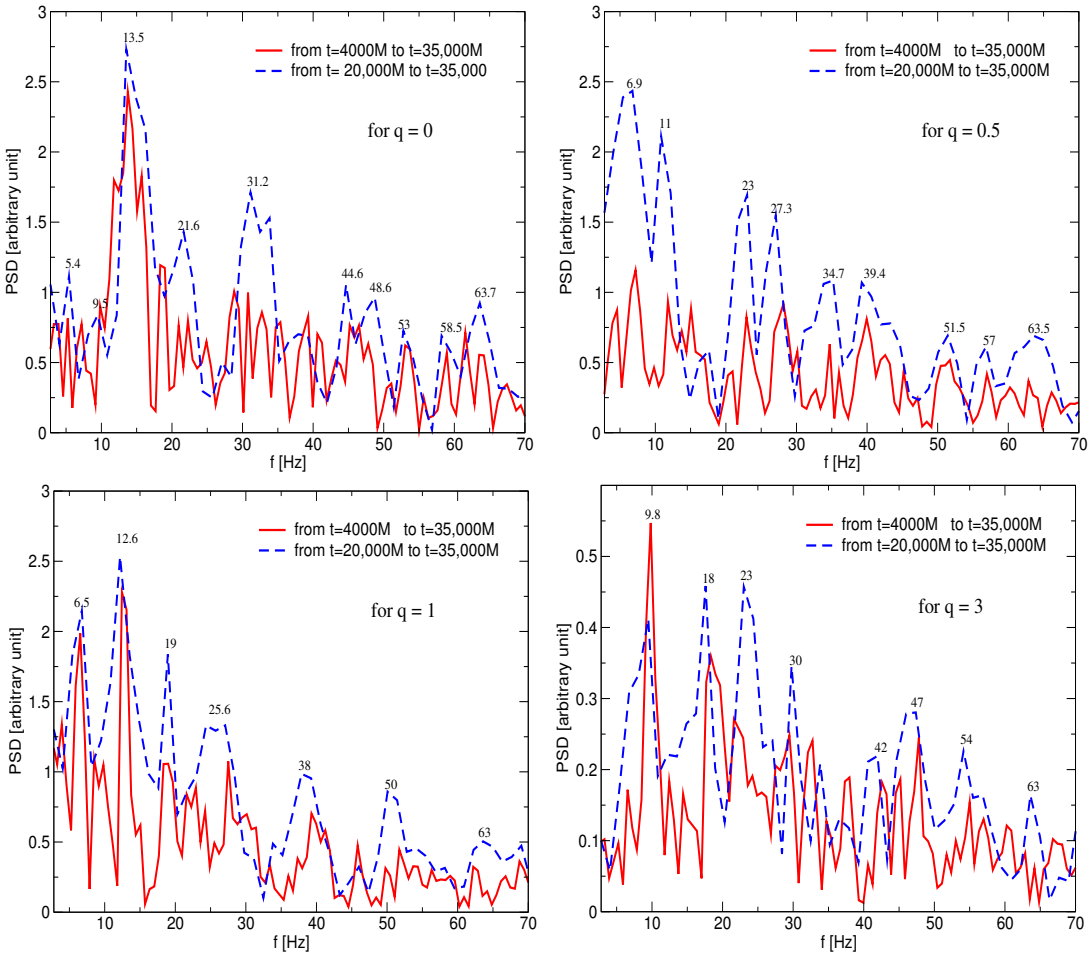

Figure 6. The behavior of the power spectrum density with respect to frequency is shown for $a/M = 0.4$ after reaching steady-state conditions. A straight line is obtained from the PSD of the mass accretion rate, seen in Figure 5, throughout the simulation immediately after reaching stability, while a dashed line is obtained from the PSD of the mass accretion rate after $t = 20{,}000\ M$. As seen, the resulting fundamental modes and their nonlinear couplings generate persistent QPOs. The first and second genuine modes are different, as are the subsequent non-linear couplings. However, in all cases presented, the formation of 1:2:3... ratios is observed.

5. BHL Accretion around a Rapidly Rotating Black Hole in Hartle–Thorne Gravity: $a/M = 0.9$

The Hartle–Thorne metric is obtained by extending the Schwarzschild metric to include the rotation parameter. In mathematical terms, this extension is made under

the assumption that the rotation parameter is much less than the speed of light. Therefore, the theory may not fully represent models of rapidly rotating black holes [47,52]. Although Hartle–Thorne gravity is suitable for describing the spacetime around slowly rotating black holes, modeling the structure of the shock cone formed by BHL accretion for rapidly rotating black holes would add scientific richness to the literature. Such modeling can help us better understand the dynamics of rapidly rotating black holes. The shock cone around a rapidly rotating black hole can be examined by comparing it with the Kerr metric or slowly rotating Hartle–Thorne black holes. This comparison can reveal the effects of black hole rotation speeds along with the quadrupole moment on the complex observed astrophysical phenomena. In particular, studying the similarities and differences between QPOs in rapidly and slowly rotating black holes can lead to a better understanding of these complex phenomena. Comparing the QPO formations within shock waves of slowly rotating black holes and Kerr black holes can provide important information about the origin and nature of these oscillations. This information, especially in the interpretation of observational data such as X-ray timings, can be useful. A detailed analysis of these dynamic structures around black holes can make significant contributions to testing the predictions of General Relativity and understanding the complex processes around black holes.

5.1. Dynamics of Shock Cones around the Hartle–Thorne Black Hole

The structure of the cone formed around the rapidly rotating Hartle–Thorne black hole, as shown in Figure 7, and its dependence on the quadrupole parameter have been revealed. Here, at $r = 3.88\ M$, the rest-mass density of the shock cone and the opening angle of the cone have been plotted for different values of q. It can be observed that the obtained results are similar to those for the slow-rotating black hole model presented in Section 4. It is clearly seen that the only difference is the larger opening angle in the rapidly rotating black hole, indicating that the black hole rotation parameter more prominently affects the cone.

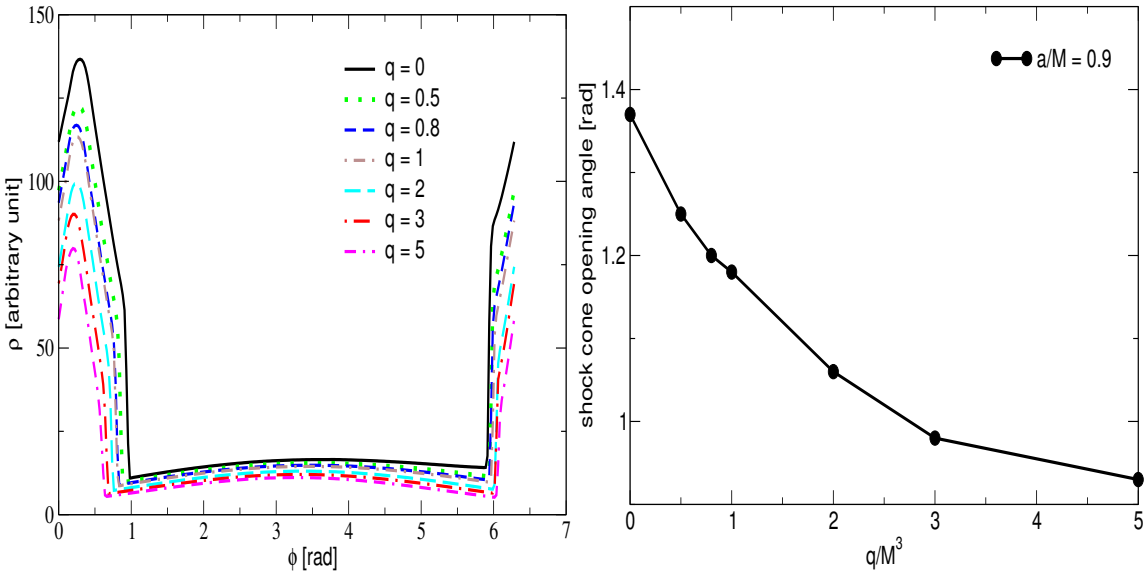

Figure 7. Same as Figure 3, but for $a/M = 0.9$.

Analogous to Section 4, the variations in radial and azimuthal velocities dependent on the quadrupole parameter are plotted in Figure 8. It has been observed that the results exhibit similarities with the cone structure formed around the slowly rotating black hole. As previously mentioned, the influence of the black hole rotation parameter on the dynamic structure of the cone near the black hole horizon is clearly evident. This influence, coupled with the changing opening angle of the cone, means that the QPO frequencies around the black hole would display different behaviors.

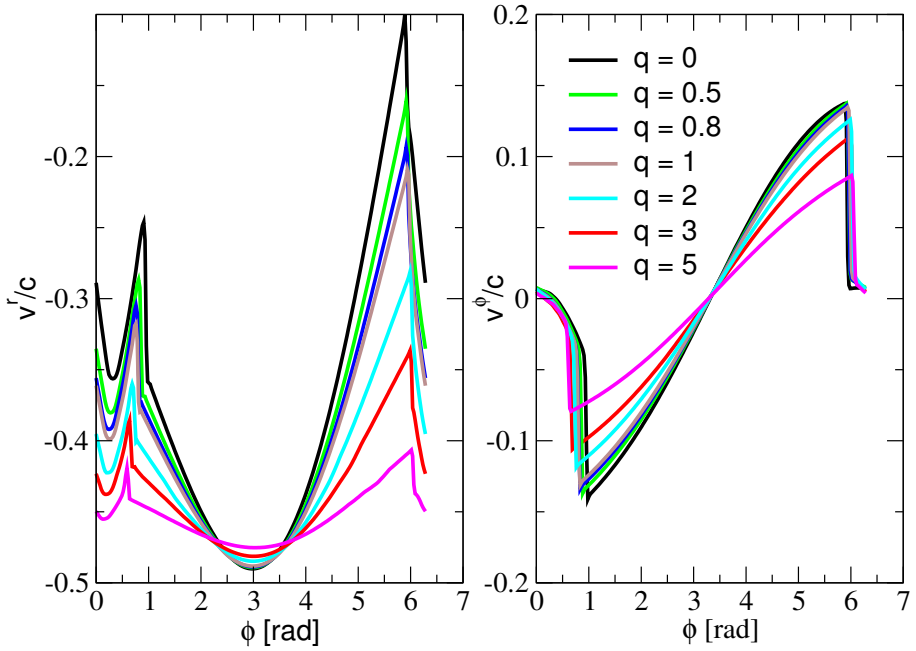

Figure 8. Same as Figure 4, but for $a/M = 0.9$.

5.2. The Shock Cone Instability around the Hartle–Thorne Black Hole

To understand the instability behavior of the shock cone, reveal its oscillation attribute, and determine the saturation time, Figure 9 depicts the mass accretion rate and the time evolution of mode power in the case of a rapidly rotating black hole, $a/M = 0.9$, similar to the model around a slow-rotating black hole discussed earlier in Section 4. Although the instability behaviors of the shock cone appear similar in both slow- and fast-rotating black hole scenarios, especially for large quadrupole parameters ($q > 2$), it is observed that the shock cone exhibits strong instability even after reaching a steady state. This suggests that, particularly for large q values, the oscillations trapped within the cone could be strongly formed and excited even after the cone reaches a steady state. This could enhance their observability, and the oscillation modes obtained for these large q values can be used to explain observational results.

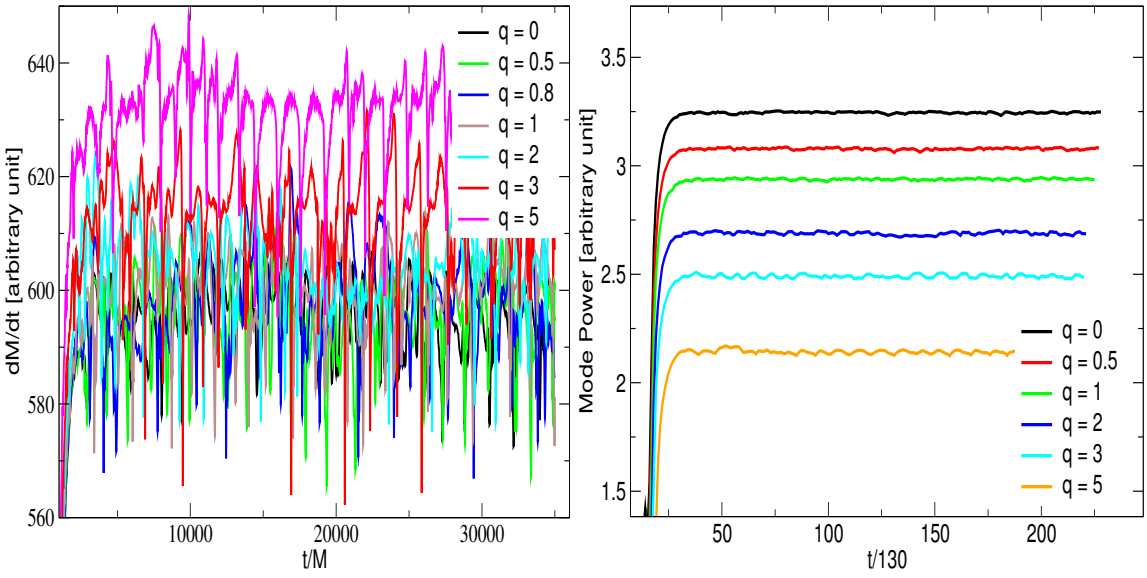

Figure 9. Same as Figure 5, but for $a/M = 0.9$.

5.3. QPOs around the Hartle–Thorne Black Hole

A rapidly spinning Hartle–Thorne black hole ($a/M = 0.9$) is theoretically impossible. However, the fact that the numerically obtained results can be compared with observations and shed light on certain cases indicates the value of the studies conducted. Simultaneously, we also open a discussion area in the literature.

We examine the behavior of quasi-periodic oscillations (QPOs) for rapidly rotating black hole models. In the case of a rapidly spinning black hole, as explained in Section 4.3, two different PSDs have also been conducted for each PSD plot. This enables the determination of which peaks are transient and which ones are persistent. As depicted in Figure 9, unlike the slowly rotating case, it has been observed that for each quadrupole parameter, after reaching a steady state around a certain value, instability arises. In the slow-rotating black hole model, no instability is observed for $q > 3$. Therefore, no corresponding QPOs have formed for these cases. However, for every q value of the rapidly spinning black hole, significant instability and QPO frequencies, as shown in Figure 10, have emerged. It has been noted that the genuine modes, f_{sh} and f_{EH}, explained in Section 4.3 manifest in these models. Furthermore, nonlinear couplings and resonance conditions have led to modes occurring outside of the fundamental modes. The PSD conducted using the mass accretion rate data obtained well after the shock cone reached the steady state and the peaks indicated by the dashed line in Figure 10 are of a nature that can be compared to observations and considered persistent.

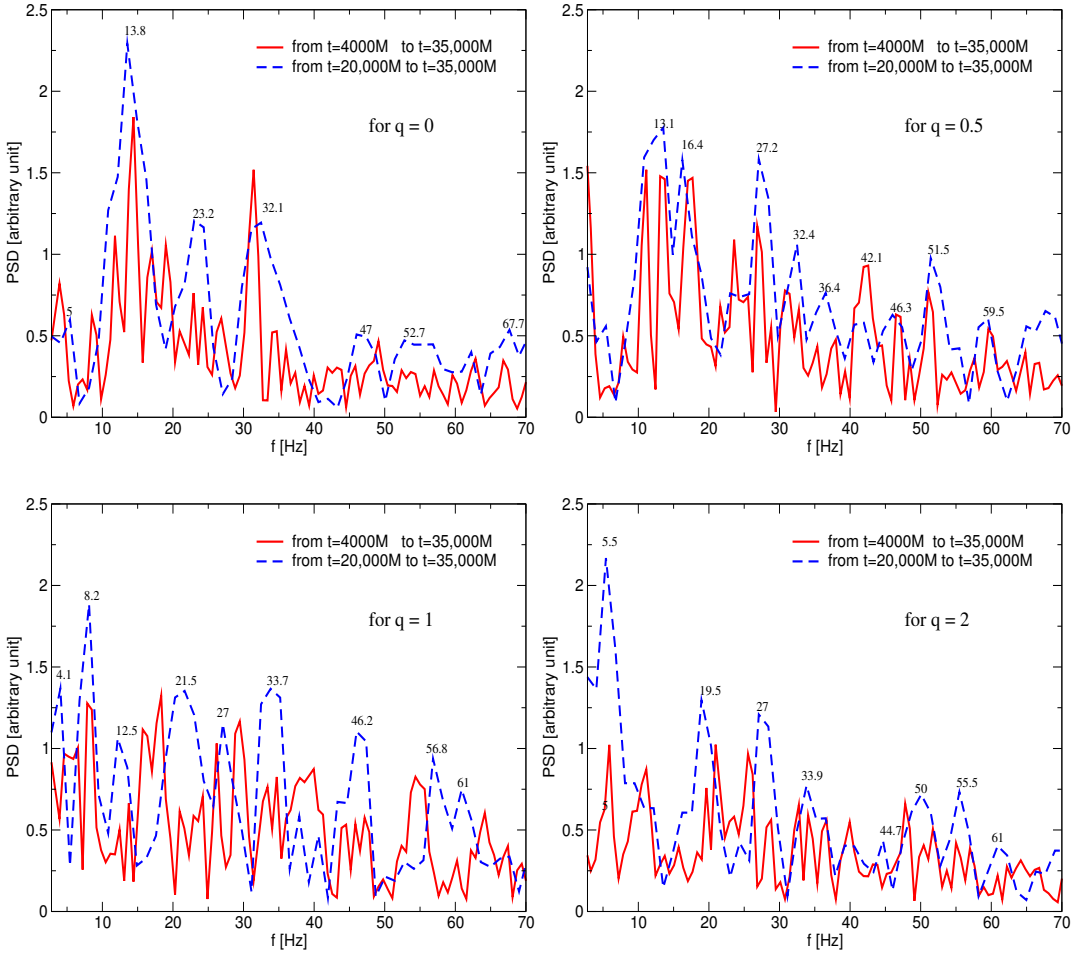

Figure 10. *Cont.*

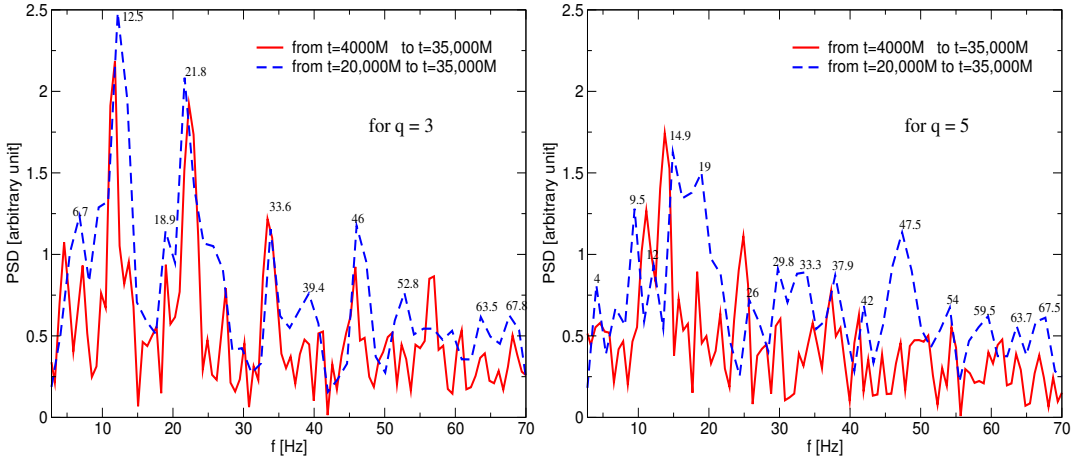

Figure 10. Same as Figure 6 but for $a/M = 0.9$.

It is natural for oscillation frequencies to differ for each q value because the azimuthal and radial QPO modes generated and excited within the cone depend entirely on the shock cone opening angle and the distance between the stagnation point and the black hole horizon. These variations are evident in Figures 7 and 8.

6. BHL Accretion around the Kerr and EGB Black Holes

Our main focus in this article is on modeling the structural behavior of the shock cone formed in Hartle–Thorne gravity due to the BHL accretion mechanism. This article investigates how Hartle–Thorne gravity theory, which is used to understand the dynamic structure of slowly rotating neutron stars, can be applied around a Hartle–Thorne black hole in various accretion scenarios using GRH. In this study, we also discuss the applicability of Hartle–Thorne gravity to rapidly rotating black holes for $a/M = 0.9$. In this context, we model the shock cone structure around Kerr and EGB black holes to make comparisons. This section reproduces how shock cones are formed for different black hole rotation parameters and EGB parameters, previously modeled numerically around non-rotating [44] and rotating [24] black holes. Later, the results produced here are compared with the models for Hartle–Thorne black holes.

Figure 11 depicts the data for non-rotating EGB and Schwarzschild black holes using different values of α. The mass accumulation rate, QPO behavior, rest-mass density at $r = 3.88\ M$, and radial and angular velocities are plotted to understand the dynamics of the shock cone. In each model, it has been found that the shock cone exhibits substantial oscillations, which persist even after the cone reaches saturation. The observed instability leads to the creation of fundamental QPO frequencies. The frequencies are determined using the mass accretion rate data obtained long after the shock cone reaches its steady state. As confirmed in Sections 4.3 and 5.3, the frequencies are a result of trapped modes within the shock cone and persist continuously. The dynamics of the cone and the oscillation modes trapped within it show clear evidence of variations at negative and positive α. This demonstrates that the variation in α significantly impacts the dynamical behavior of the shock cone around black holes in EGB gravity. Such changes in the shock cone structure and the trapped modes provide a crucial perspective on the complex physics of the cone and its interaction with the black hole, particularly in the context of EGB gravity.

Similar to Figure 11, Figure 12 presents calculations for the same physical parameters but for a rotating black hole with a spin parameter of $a/M = 0.4$ in both Kerr and EGB scenarios. Although generally similar behaviors are observed, the influence of the black hole spin parameter is particularly noticeable in the density and velocity graphs. Additionally, the calculated QPO frequencies appear more distinct and clear in this scenario. The observed harmonic ratios of 1:2:3... are also clearly visible here. These observations highlight the significant impact of the spin parameter on the physical characteristics of the shock cone and the QPO frequencies. The differences between the Kerr and EGB

models, in terms of how rotation affects their properties, are of particular interest. They provide valuable insights into the complexities of gravitational interactions in the vicinity of rotating black holes, especially in alternative theories of gravity like EGB. Such findings are crucial for advancing our understanding of high-energy astrophysical phenomena and the fundamental nature of gravity.

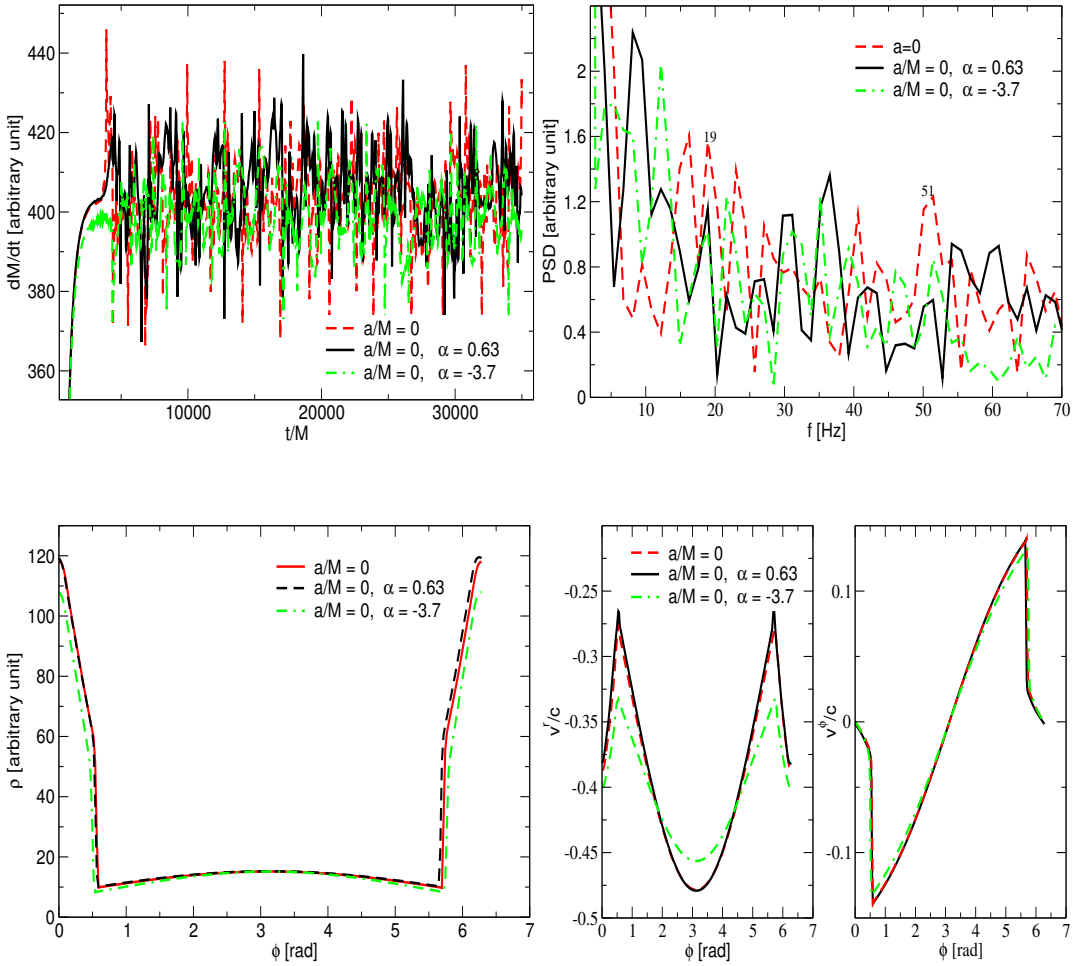

Figure 11. For $a/M = 0$, the change in the property of the shock cone in EGB gravities is shown. The mass accretion rate over time is given in the top left corner, while the power spectrum analysis is shown in the top right. The changes in the rest-mass density and the radial and azimuthal velocities in the azimuthal direction at $r = 3.88\ M$ are shown.

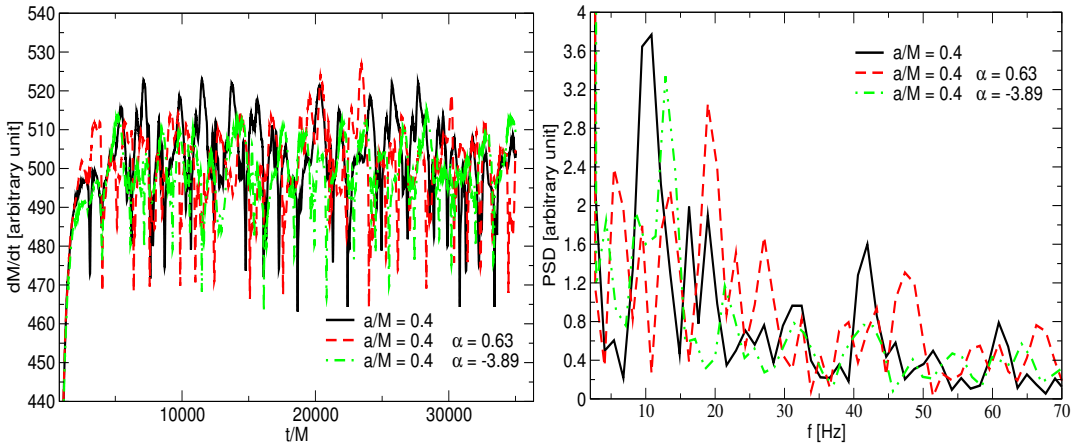

Figure 12. *Cont.*

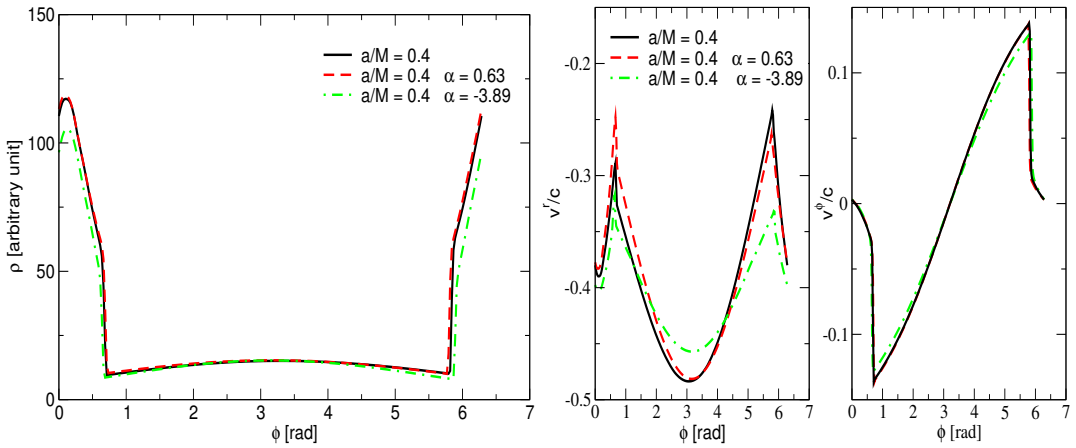

Figure 12. Same as Figure 11 but for $a/M = 0.4$.

Similar to Figures 11 and 12, Figure 13 unveils the shock cone structure and oscillation frequencies for the rapidly rotating black hole in both Kerr and EGB gravities. The impact of the black hole rotation on the structure of the shock cone is clearly observed. The QPO frequencies and their nonlinear couplings in these models have created a more complex structure. Furthermore, the influence of the α parameter on the structure of the shock cone and its oscillations is evident. This demonstrates how the rotation of the black hole significantly affects the behavior of the shock cone and the resulting QPO frequencies. In the case of rapidly rotating black holes, these results provide a deeper understanding of the complex interactions between the black hole spin, the shock cone structure, and QPOs. Such studies are crucial for understanding astrophysical phenomena in strong gravitational environments.

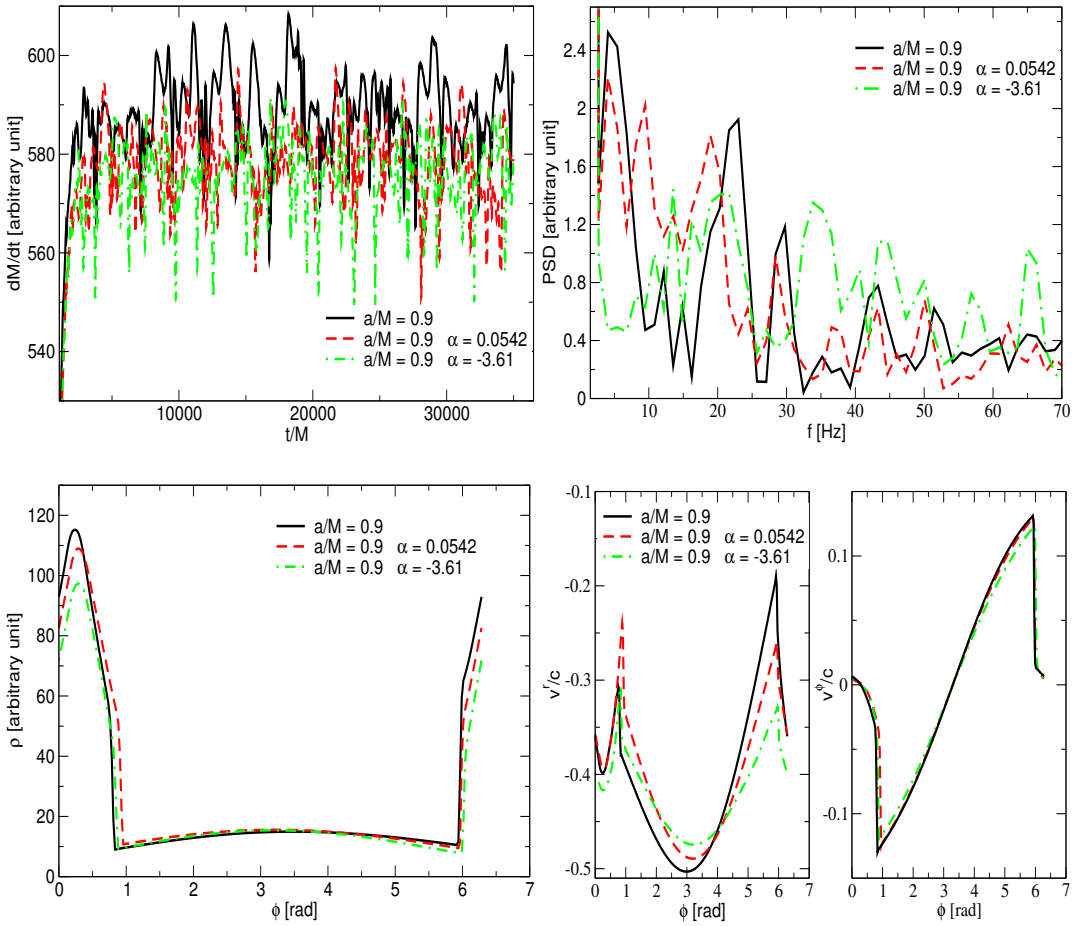

Figure 13. Same as Figure 11 but for $a/M = 0.9$.

7. Comparison of Hartle–Thorne Gravity with Schwarzschild, Kerr, and EGB Gravities

Figure 14 illustrates the changes in the density of the cone and its contour lines to investigate the effect of the Hartle–Thorne spacetime metric on the shock cone near the black hole horizon and to compare the results with those of a Kerr black hole. The snapshots in the top row show the dynamic structure of the shock cone close to the black hole horizon for both slowly and rapidly rotating Kerr black holes. Although the frame-dragging effect is not clearly visible due to the inner boundary of the computational area being at $r = 3.8\ M$, this effect slightly appears in the case of $a/M = 0.4$ and is more distinct at $a/M = 0.9$. In this study, we investigated the changes in the dynamic structure of the shock cone using Hartle–Thorne in conjunction with EGB gravity. Within the framework of EGB gravity, we compared the extreme states of the EGB coupling constant with those of Hartle–Thorne, Schwarzschild, and Kerr black holes. In the extreme case where $\alpha \sim -3.7$, as observed in Donmez [24], the black hole horizon is located at $r \sim 3.5\ M$. To ensure a reliable comparison, we set the inner boundary of the calculation domain at $r = 3.8\ M$ in all models.

At $a/M = 0.9$, the shock waves of the cone are warped due to the black hole rotation. The effect of rotation is also visible in the contour lines within the shock cone. The Hartle–Thorne gravity, without the quadrupole parameter, affects the structure of the shock cone, as seen in the middle row of the same figure. The same behaviors observed in the Kerr models are also exhibited. The bottom row of Figure 14 shows the changes in the dynamic structure of the shock cone when the quadrupole parameter is $q = 5$. Here, it is found that the quadrupole parameter reduces the shock opening angle of the cone and causes a greater suppression of contour lines. In other words, the contour lines have become more curved, and the ellipticity ratio has significantly increased. This led to a noticeable change within the cone. This is an expected result, as the quadrupole introduces a more elliptical shape by suppressing the polar geometry of spherical symmetry. This change causes variations in the frequencies of the QPO modes trapped within the shock cone. It also triggers a chaotic structure within the cone, facilitating the observation of new frequencies through changes in the behaviors of nonlinear couplings. This chaotic structure allows for the observation of new frequencies resulting from these nonlinear interactions. Additionally, the velocity vector plots also show how the flow velocity of matter changes, especially in the region near the black hole horizon inside the cone. This would affect the formation of QPOs. This situation is clearly observed in Figures 6 and 10 as well.

As previously discussed, the shock cone formed as a result of BHL accretion traps oscillation modes within the cone, leading to the excitation of these modes. Observing these phenomena helps reveal the physical characteristics of the central black hole. Figure 15 compares the fundamental mode frequencies and their nonlinear couplings excited by the shock cones around slowly rotating (left graph, $a = 0.4$) and rapidly rotating (right graph, $a = 0.9$) black holes across various gravities. In the case of the slowly rotating black hole, the same fundamental mode frequencies, $f_1 = 5.5$ Hz, $f_2 = 11$ Hz, and $f_3 = 19$ Hz, occur in Kerr, EGB, and Hartle–Thorne gravities. However, the frequencies resulting from the nonlinear coupling of these two fundamental modes show variations in different gravities. This could be an important finding, indicating how different gravitational theories can produce varied effects on the dynamics of matter surrounding dense astrophysical objects like black holes. Similarly, calculations have also been made for the fundamental modes trapped by shock cones around rapidly rotating black holes. As seen in the right graph, the fundamental mode frequencies are excited at $q_1 = 4.2$ Hz, $q_2 = 13$ Hz, and $q_3 = 20.4$ Hz. Almost the same modes occur in all three gravitational models. However, as with the slowly rotating black hole model, the nonlinear couplings of these modes differ from one another.

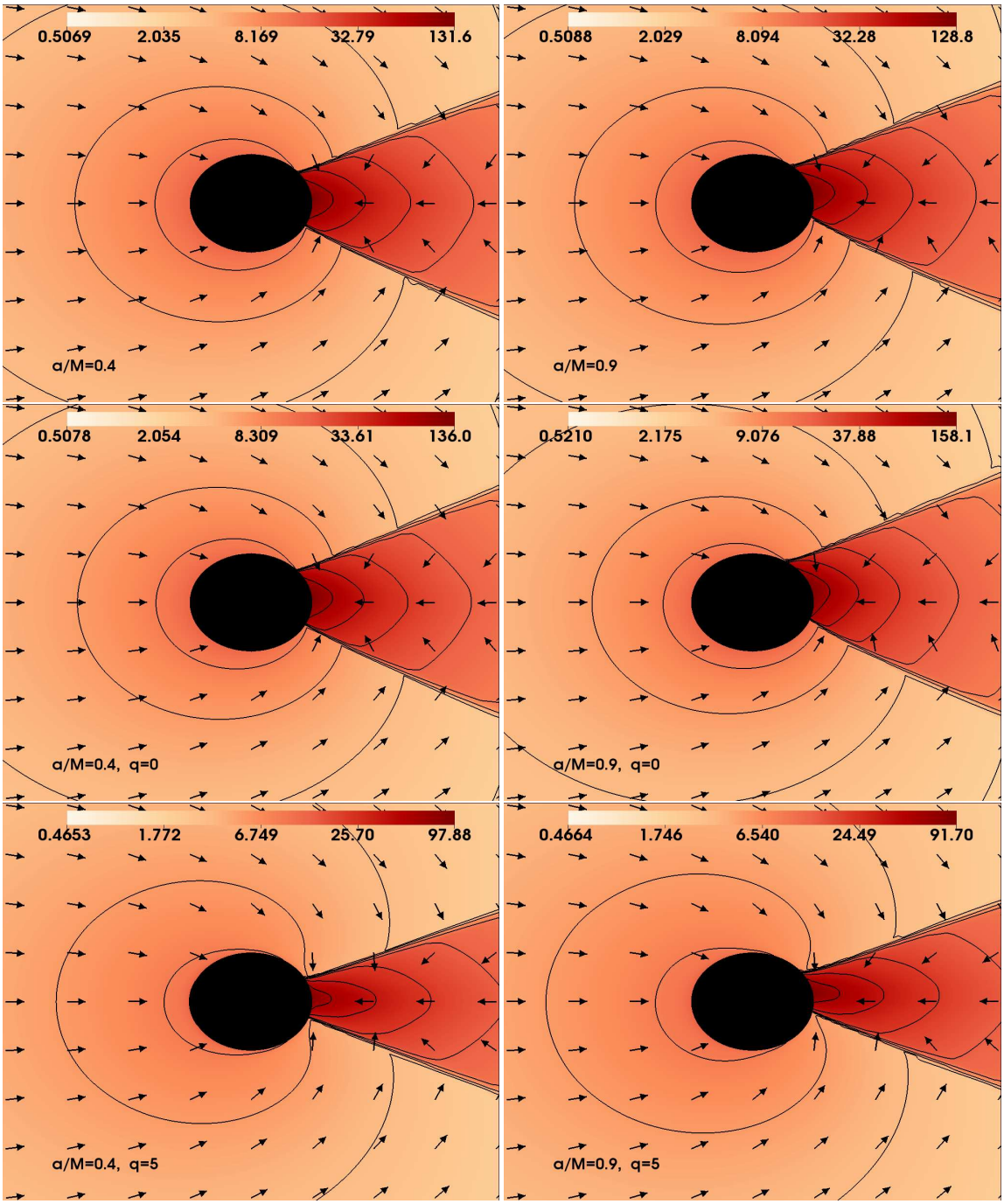

Figure 14. Same as Figure 2 but for the models of slowly and rapidly rotating black holes. The dynamic structure of the shock cones formed around the Kerr and Hartle–Thorne black holes is shown. We focus on the region near the horizon to see more details. The effect of q on the structure of the cone has been clearly demonstrated.

The shock cone formed around the black hole leads to the confinement of excited QPO modes due to the interaction between the shock cone and the black hole, causing these modes to be excited more intensely. Additionally, chaotic behavior within the shock cone results in the emergence of new nonlinear oscillation modes. These modes can be utilized to explain certain QPO frequencies observed in astronomical data. Figure 16 illustrates the general behavior of the shock cone around a rapidly rotating Hartle–Thorne black hole, demonstrating its similarity to the behavior around a slowly rotating Hartle–Thorne black hole. In both cases of rotation parameters, the opening angle of the shock cone

exhibits similar behavior depending on the quadrupole parameter. It is evident that the primary differences arise from the rotation parameter rather than the quadrupole parameter. Therefore, investigating the structure of the shock cone around a rapidly rotating Hartle–Thorne black hole contributes additional insights to the literature and can be used to explain some of the observed phenomena. The numerical results obtained in this study suggest the possible existence of a rapidly rotating Hartle–Thorne black hole.

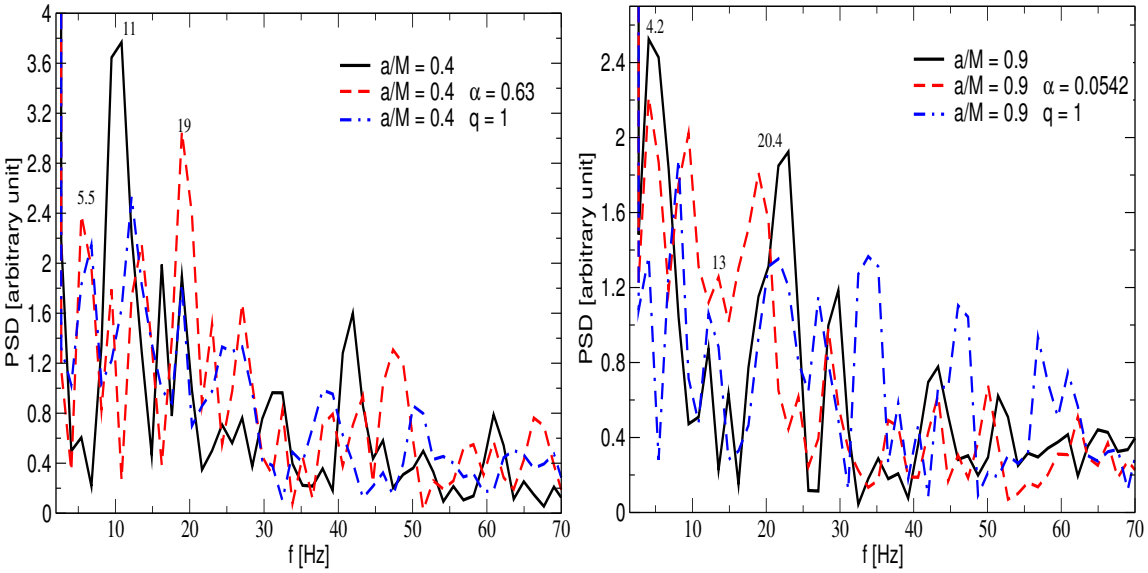

Figure 15. Comparison of QPO frequencies stimulated by the accreting matter around the slow- (**the left part**) and fast-rotating (**the right part**) black holes in Kerr, EGB, and Hartle–Thorne gravities. The same fundamental frequencies have been observed in all three gravitational models, but differences in the frequencies resulting from nonlinear interactions have been detected among these models. This provides an important clue as to how different gravitational theories can create varied effects on the dynamics of matter surrounding dense astrophysical objects like black holes.

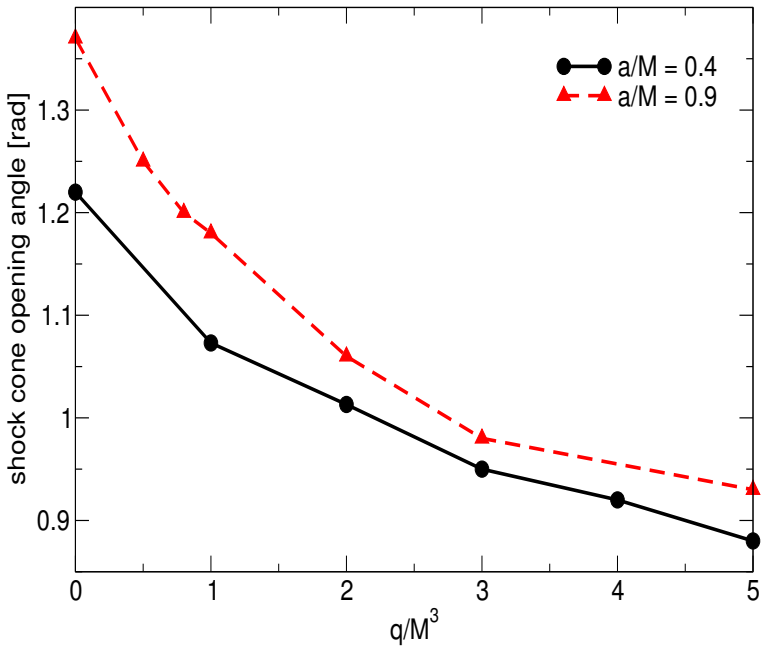

Figure 16. The variation in the opening angle of the shock cone around the slowly and rapidly rotating black holes depending on the quadrupole parameter. It has been observed that as the quadrupole parameter increases and the black hole rotation parameter decreases, the opening angle decreases. This directly affects the QPO frequencies.

8. Discussion and Conclusions

In this article, we reveal the dynamic structure of the shock cone formed around the Hartle–Thorne black hole as a result of BHL accretion and examine how the trapped QPO frequencies within the cone depend on various parameters, such as the black hole spin (a/M) and the quadrupole parameter (q). Although Hartle–Thorne gravity is theoretically defined for slowly rotating black hole models, we have also numerically modeled scenarios around rapidly spinning Hartle–Thorne black holes, further contributing to the literature and sparking new discussions in this field. Furthermore, to compare the results obtained from Hartle–Thorne gravity with those from different gravitational models, we have also modeled the same problem within the frameworks of Schwarzschild, Kerr, and EGB gravities.

The numerical simulations show that the opening angle of the shock cone around the slowly rotating Hartle–Thorne black hole, the instability of the shock cone, the amount of matter accreting within the cone, and the intensity of the shock waves are not only dependent on the rotation parameter of the black hole but also strongly linked to the quadrupole parameter of Hartle–Thorne gravity. It is observed that as the quadrupole parameter q increases, the opening angle of the shock cone decreases, and more matter falls into the black hole. This implies that nonlinear behaviors become more pronounced as q takes larger values. Additionally, the instability behavior is found to decrease after the quadrupole parameter exceeds 2. These instabilities, being the source of oscillation modes that form or are trapped within the cone, lead to the creation of genuine QPO frequencies and their superposition, resulting in new frequencies. The fundamental QPO frequencies are the result of the behavior of matter oscillating in the azimuthal and radial directions due to pressure differences. Because the matter trapped within the shock cone begins to undergo these oscillations, it generates the fundamental QPO genuine modes. These modes generally correspond to the most prominent first two peaks in the PSD graph. The decrease in the intensity of these instabilities leads to a reduction in the strength of QPOs and the disappearance of potential new frequencies or ratios. This means that in situations where $q > 2$, the number of observable frequencies is diminished.

According to theory, Hartle–Thorne gravity describes the spacetime around slowly rotating black holes. In our study, we also numerically address the scenario where the black hole is rapidly spinning, revealing how this affects the structure of the shock cone around the black hole [49]. Similar to the model for a slowly rotating black hole, the structure of the shock cone can be comparable. However, the shock cone is observed to be more warped due to the influence of the black hole rotation parameter. It is shown that shock cone instability is very strong at every value of the quadrupole parameter, a behavior not observed in models of slowly rotating black holes. This suggests that the observability of QPO frequencies in the interaction of the rapidly spinning Hartle–Thorne black hole with the shock cone could be higher compared to the slowly rotating models. However, it is important to mention that the model for a rapidly spinning black hole is exclusively a numerical approximation. It could be used to explain some observational results and may open new discussions in the field.

The results obtained from Hartle–Thorne gravity are compared with those from Kerr and EGB gravities. We focus on the impact of the quadrupole parameter on the shock cone structure and the resulting QPO frequencies. It is observed that the QPO modes and their nonlinear couplings exhibit different behaviors at different values of the quadrupole parameter. This finding can be used to explain certain observed black hole sources whose physical mechanisms remain unexplained. Furthermore, the comparison reveals that the quadrupole parameter suppresses the density within the shock cone and leads to a more elliptical structure. Such effects provide sufficient reasons for the emergence of different oscillation frequencies. This insight enhances our understanding of black hole physics, especially in the context of rapidly rotating black holes and their complex interactions with the accretion disk.

As a result of the conducted PSDs for both slowly and rapidly rotating black holes, it has been concluded that the majority of frequencies present in all gravities are persistent. Through PSDs conducted at different time intervals, it has been found that genuine modes trapped within the shock cone and their nonlinear coupling occur at the same frequency. This implies that the shock cone, which we have characterized based on numerical modeling and the parameters defining the gravity, serves as a physical mechanism for the formation of QPO frequencies. This mechanism, as previously mentioned in various studies [16,42,60,61], can be utilized to explain QPO data observed from different sources. Thus, the physical characteristics of the source, such as mass and rotation parameters, can be determined. The obtained results can then be compared with observations.

Finally, it has been observed in all models that a 1:2:3... ratio forms after the shock cone reaches its saturation point. These ratios indicate a harmonic relationship among QPO frequencies. The presence of this harmonic relationship suggests the existence of a physical mechanism or condition in the regions close to the black hole horizon. Additionally, these harmonics result from nonlinear couplings, which in turn indicate the presence of nonlinear behavior. The study further shows that the quadrupole parameter of the Hartle–Thorne black hole definitely triggers nonlinear phenomena. We reach this conclusion from the simulations conducted. The implications of such results are significant in the field of astrophysics. It also points to complex interactions in the vicinity of black holes, which are particularly influenced by the geometry and the gravitational field defined by the Hartle–Thorne metric. Understanding these nonlinear behaviors and their effects, such as the quadrupole parameter, is crucial for developing more accurate models around black holes. This knowledge not only helps in explaining the observed phenomena around black holes but also enriches the theoretical framework of our understanding of these objects.

Author Contributions: Conceptualization, methodology and investigation, O.D. and F.D.; software, validation, formal analysis, resources, data curation, writing—original draft preparation, writing—review and editing, and visualization, O.D. and F.D. All authors have read and agreed to the published version of the manuscript.

Funding: This research received no external funding.

Data Availability Statement: The data used in the article are entirely composed of data obtained by running our own program, which solves the General Relativistic Hydrodynamics Equations, on a High-Performance Computer. Data can be sent to the requested people through private communication.

Acknowledgments: All simulations were performed using the Phoenix High Performance Computing facility at the American University of the Middle East (AUM), Kuwait. In order to improve the linguistic quality and to correct grammatical errors in the paper, AI has been used. I would also like to thank the anonymous referees for their contributions to improving the quality of the paper.

Conflicts of Interest: The authors declare no conflicts of interest.

References

1. Remillard, R.A.; McClintock, J.E.; Orosz, J.A.; Levine, A.M. The X-ray Outburst of H1743-322 in 2003: High-Frequency QPOs with a 3:2 Frequency Ratio. *Astrophys. J.* **2006**, *637*, 1002–1009. [CrossRef]
2. Motta, S.E. Quasi periodic oscillations in black hole binaries. *Astron. Nachrichten* **2016**, *337*, 398. [CrossRef]
3. Belloni, T.M.; Sanna, A.; Méndez, M. High-frequency quasi-periodic oscillations in black hole binaries. *Mon. Not. R. Astron. Soc.* **2012**, *426*, 1701–1709. [CrossRef]
4. Strohmayer, T.E. Discovery of a Second High-Frequency Quasi-periodic Oscillation from the Microquasar GRS 1915+105. *Astrophys. J.* **2001**, *554*, L169–L172. [CrossRef]
5. Homan, J.; Klein-Wolt, M.; Rossi, S.; Miller, J.M.; Wijnands, R.; Belloni, T.; van der Klis, M.; Lewin, W.H.G. High-Frequency Quasi-periodic Oscillations in the Black Hole X-Ray Transient XTE J1650-500. *Astrophys. J.* **2003**, *586*, 1262–1267. [CrossRef]
6. Motta, S.E.; Belloni, T.M. Rethinking the 67 Hz QPO in GRS 1915+105: Type-C QPOs at the innermost stable circular orbit. *arXiv* **2023**, arXiv:2307.00867. [CrossRef]
7. Belloni, T.M.; Stella, L. Fast Variability from Black-Hole Binaries. *Phys. Accretion Black Holes* **2014**, *183*, 43–60. [CrossRef]
8. Kato, S. Excitation of Non-Axisymmetric g-MOde Oscillations by Corotation Resonance in Thin Relativistic Disks. *Publ. Astron. Soc. Jpn.* **2002**, *54*, 39–51. [CrossRef]

9. Chakrabarti, S.K.; Acharyya, K.; Molteni, D. Quasi-Periodic Oscillations in Numerical Simulation of Accretion Flows Around Black Holes. *arXiv* **2002**, arXiv:astro-ph/0211516. [CrossRef]
10. Montero, P.J.; Rezzolla, L.; Yoshida, S. Oscillations of vertically integrated relativistic tori-II. Axisymmetric modes in a Kerr space-time. *Mon. Not. R. Astron. Soc.* **2004**, *354*, 1040–1052. [CrossRef]
11. Aoki, S.I.; Koide, S.; Kudoh, T.; Nakayama, K.; Shibata, K. Quasi-periodic Inward Shock Formations in the System of a Black Hole and an Accretion Disk and Application to Quasi-periodic Oscillations in Galactic Black Hole Candidates. *Astrophys. J.* **2004**, *610*, 897–912. [CrossRef]
12. Schnittman, J.D.; Rezzolla, L. Quasi-periodic Oscillations in the X-Ray Light Curves from Relativistic Tori. *Astrophys. J.* **2006**, *637*, L113–L116. [CrossRef]
13. Kološ, M.; Shahzadi, M.; Stuchlík, Z. Quasi-periodic oscillations around Kerr-MOG black holes. *Eur. Phys. J. C* **2020**, *80*, 133. [CrossRef]
14. Ruffert, M. Three-dimensional Hydrodynamic Bondi-Hoyle Accretion. I. Code Validation and Stationary Accretors. *Astrophys. J.* **1994**, *427*, 342. [CrossRef]
15. Ruffert, M.; Arnett, D. Three-dimensional Hydrodynamic Bondi-Hoyle Accretion. II. Homogeneous Medium at Mach 3 with gamma = 5/3. *Astrophys. J.* **1994**, *427*, 351. [CrossRef]
16. Dönmez, O.; Zanotti, O.; Rezzolla, L. On the development of quasi-periodic oscillations in Bondi-Hoyle accretion flows. *Mon. Not. R. Astron. Soc.* **2011**, *412*, 1659–1668. [CrossRef]
17. Dönmez, O. Relativistic simulation of flip-flop instabilities of Bondi-Hoyle accretion and quasi-periodic oscillations. *Mon. Not. R. Astron. Soc.* **2012**, *426*, 1533–1545. [CrossRef]
18. Dönmez, O. On the development of the Papaloizou-Pringle instability of the black hole-torus systems and quasi-periodic oscillations. *Mon. Not. R. Astron. Soc.* **2014**, *438*, 846–858. [CrossRef]
19. Koyuncu, F.; Dönmez, O. Numerical simulation of the disk dynamics around the black hole: Bondi-Hoyle accretion. *Mod. Phys. Lett. A* **2014**, *29*, 1450115. [CrossRef]
20. Cruz-Osorio, A.; Lora-Clavijo, F.D. Non-axisymmetric relativistic wind accretion with velocity gradients on to a rotating black hole. *Mon. Not. R. Astron. Soc.* **2016**, *460*, 3193–3201. [CrossRef]
21. Lora-Clavijo, F.D.; Cruz-Osorio, A.; Moreno Méndez, E. Relativistic Bondi-Hoyle-Lyttleton Accretion onto a Rotating Black Hole: Density Gradients. *Astrophys. J. Suppl. Ser.* **2015**, *219*, 30. [CrossRef]
22. Ohsugi, Y. Bondi–Hoyle–Lyttleton accretion flow revisited: Numerical simulation of unstable flow. *Astron. Comput.* **2018**, *25*, 44–51. [CrossRef]
23. Lora-Clavijo, F.D.; Guzmán, F.S. Axisymmetric Bondi-Hoyle accretion on to a Schwarzschild black hole: Shock cone vibrations. *Mon. Not. R. Astron. Soc.* **2013**, *429*, 3144–3154. [CrossRef]
24. Donmez, O. Dynamical evolution of the shock cone around 4D Einstein-Gauss Bonnet rotating black hole. *Phys. Lett. B* **2022**, *827*, 136997. [CrossRef]
25. Donmez, O. Perturbing the Stable Accretion Disk in Kerr and 4-D Einstein-Gauss-Bonnet Gravities:Comprehensive Analysis of Instabilities and Dynamics. *arXiv* **2023**, arXiv:2310.13847. [CrossRef]
26. van der Klis, M. Millisecond Oscillations in X-ray Binaries. *Annu. Rev. Astron. Astrophys.* **2000**, *38*, 717–760. [CrossRef]
27. Smith, K.L.; Tandon, C.R.; Wagoner, R.V. Confrontation of Observation and Theory: High-frequency QPOs in X-Ray Binaries, Tidal Disruption Events, and Active Galactic Nuclei. *Astrophys. J.* **2021**, *906*, 92, [CrossRef]
28. Remillard, R.A.; Morgan, E.H.; McClintock, J.E.; Bailyn, C.D.; Orosz, J.A. RXTE Observations of 0.1-300 HZ Quasi-periodic Oscillationsin the Microquasar GRO J1655-40. *Astrophys. J.* **1999**, *522*, 397–412. [CrossRef]
29. Motta, S.E.; Belloni, T.M.; Stella, L.; Muñoz-Darias, T.; Fender, R. Precise mass and spin measurements for a stellar-mass black hole through X-ray timing: The case of GRO J1655-40. *Mon. Not. R. Astron. Soc.* **2014**, *437*, 2554–2565. [CrossRef]
30. Tchekhovskoy, A.; Narayan, R.; McKinney, J.C. Efficient generation of jets from magnetically arrested accretion on a rapidly spinning black hole. *Mon. Not. R. Astron. Soc.* **2011**, *418*, L79–L83. [CrossRef]
31. Done, C.; Jin, C. The mass and spin of the extreme Narrow Line Seyfert 1 Galaxy 1H 0707-495 and its implications for the trigger for relativistic jets. *Mon. Not. R. Astron. Soc.* **2016**, *460*, 1716–1724. [CrossRef]
32. Reynolds, C.S. Observing black holes spin. *Nat. Astron.* **2019**, *3*, 41–47. [CrossRef]
33. Feng, Y.; Zhao, X.; Li, Y.; Gou, L.; Jia, N.; Liao, Z.; Wang, Y. The Spin of New Black Hole Candidate: MAXI J1803-298 Observed by NuSTAR and NICER. *arXiv* **2021**, arXiv:2112.02794. [CrossRef]
34. Wu, H.; Wang, W.; Sai, N.; Zhu, H.; Chen, J. A moderate spin for the black hole in X-ray binary MAXI J1348-630 revealed by Insight-HXMT. *Mon. Not. R. Astron. Soc.* **2023**, *522*, 4323–4331. [CrossRef]
35. Bondi, H.; Hoyle, F. On the mechanism of accretion by stars. *Mon. Not. R. Astron. Soc.* **1944**, *104*, 273. [CrossRef]
36. Bondi, H. On spherically symmetrical accretion. *Mon. Not. R. Astron. Soc.* **1952**, *112*, 195. [CrossRef]
37. Edgar, R. A review of Bondi-Hoyle-Lyttleton accretion. *New Astron. Rev.* **2004**, *48*, 843–859. [CrossRef]
38. Giulini, D. Luciano Rezzolla and Olindo Zanotti: Relativistic hydrodynamics. *Gen. Relativ. Gravit.* **2015**, *47*, 3. [CrossRef]
39. Foglizzo, T.; Galletti, P.; Ruffert, M. A fresh look at the unstable simulations of Bondi-Hoyle-Lyttleton accretion. *Astron. Astrophys.* **2005**, *435*, 397–411. [CrossRef]
40. Zanotti, O.; Roedig, C.; Rezzolla, L.; Del Zanna, L. General relativistic radiation hydrodynamics of accretion flows-I. Bondi-Hoyle accretion. *Mon. Not. R. Astron. Soc.* **2011**, *417*, 2899–2915. [CrossRef]

41. Cruz-Osorio, A.; Rezzolla, L. Common-envelope Dynamics of a Stellar-mass Black Hole: General Relativistic Simulations. *Astrophys. J.* **2020**, *894*, 147. [CrossRef]
42. Cruz-Osorio, A.; Rezzolla, L.; Lora-Clavijo, F.D.; Font, J.A.; Herdeiro, C.; Radu, E. Bondi-Hoyle-Lyttleton accretion onto a rotating black hole with ultralight scalar hair. *J. Cosmol. Astropart. Phys.* **2023**, *2023*, 057. [CrossRef]
43. Penner, A.J. Ultrarelativistic Bondi–Hoyle accretion–I. Axisymmetry. *Mon. Not. R. Astron. Soc.* **2012**, *428*, 2171–2184. [CrossRef]
44. Donmez, O. Bondi-Hoyle accretion around the non-rotating black hole in 4D Einstein-Gauss-Bonnet gravity - Bondi-Hoyle around EGB black hole. *Eur. Phys. J. C* **2021**, *81*, 113. [CrossRef]
45. Hartle, J.B. Slowly Rotating Relativistic Stars. I. Equations of Structure. *Astrophys. J.* **1967**, *150*, 1005. [CrossRef]
46. Bini, D.; Geralico, A.; Luongo, O.; Quevedo, H. Generalized Kerr spacetime with an arbitrary mass quadrupole moment: Geometric properties versus particle motion. *Class. Quantum Gravity* **2009**, *26*, 225006. [CrossRef]
47. Hartle, J.B.; Thorne, K.S. Slowly Rotating Relativistic Stars. II. Models for Neutron Stars and Supermassive Stars. *Astrophys. J.* **1968**, *153*, 807. [CrossRef]
48. Abramowicz, M.A.; Almergren, G.J.E.; Kluzniak, W.; Thampan, A.V. The Hartle-Thorne circular geodesics. *arXiv* **2003**, arXiv:gr–qc/0312070. [CrossRef]
49. Urbancová, G.; Urbanec, M.; Török, G.; Stuchlík, Z.; Blaschke, M.; Miller, J.C. Epicyclic Oscillations in the Hartle-Thorne External Geometry. *Astrophys. J.* **2019**, *877*, 66. [CrossRef]
50. Kurmanov, Y.; Muccino, M.; Boshkayev, K.; Konysbayev, T.; Luongo, O.; Quevedo, H.; Urazalina, A. Accretion disk in the Hartle-Thorne spacetime. *arXiv* **2023**, arXiv:2306.15050. [CrossRef]
51. Cromartie, H.T.; Fonseca, E.; Ransom, S.M.; Demorest, P.B.; Arzoumanian, Z.; Blumer, H.; Brook, P.R.; DeCesar, M.E.; Dolch, T.; Ellis, J.A.; et al. Relativistic Shapiro delay measurements of an extremely massive millisecond pulsar. *Nat. Astron.* **2020**, *4*, 72–76. [CrossRef]
52. Misner, C.W.; Thorne, K.S.; Wheeler, J.A. *Gravitation*; W. H. Freeman and Company: New York, NY, USA, 1977; Volume I.
53. Glavan, D.; Lin, C. Einstein-Gauss-Bonnet Gravity in Four-Dimensional Spacetime. *Phys. Rev. Lett.* **2020**, *124*, 081301. [CrossRef]
54. Ghosh, S.G.; Kumar, R. Generating black holes in 4D Einstein-Gauss-Bonnet gravity. *Class. Quantum Gravity* **2020**, *37*, 245008. [CrossRef]
55. Wei, S.W.; Liu, Y.X. Testing the nature of Gauss-Bonnet gravity by four-dimensional rotating black hole shadow. *Eur. Phys. J. Plus* **2021**, *136*, 436. [CrossRef]
56. Donmez, O.; Dogan, F.; Sahin, T. Study of Asymptotic Velocity in the Bondi–Hoyle Accretion Flows in the Domain of Kerr and 4-D Einstein–Gauss–Bonnet Gravities. *Universe* **2022**, *8*, 458, [CrossRef]
57. Fernandes, P.G.S.; Carrilho, P.; Clifton, T.; Mulryne, D.J. The 4D Einstein-Gauss-Bonnet theory of gravity: A review. *Class. Quantum Gravity* **2022**, *39*, 063001. [CrossRef]
58. Font, J.A. Numerical Hydrodynamics in General Relativity. *Living Rev. Relativ.* **2000**, *3*, 2. [CrossRef] [PubMed]
59. Dönmez, O. Code Development of Three-Dimensional General Relativistic Hydrodynamics with AMR (Adaptive-Mesh Refinement) and Results from Special and General Relativistic Hydrodynamics. *Astrophys. Space Sci.* **2004**, *293*, 323–354. [CrossRef]
60. Donmez, O. Bondi-Hoyle-Lyttleton Accretion around the Rotating Hairy Horndeski Black Hole. *arXiv* **2024**, arXiv:2402.16707. [CrossRef]
61. Donmez, O. Proposing a Physical Mechanism to Explain Various Observed Sources of QPOs by Simulating the Dynamics of Accretion Disks around the Black Holes. *arXiv* **2023**, arXiv:2311.08388. [CrossRef]